buildings

MDPI

Review

Efficacy of Self-Healing Concrete for Mitigating Reinforcement Corrosion: A Critical Review of Transport Properties and Electrochemical Performance

Segun J. Osibodu [1,*], Daniel D. Akerele [2] and Gideon O. Bamigboye [3]

[1] Department of Civil Engineering and Environmental Engineering, Auburn University, Auburn, AL 36849, USA
[2] Department of Construction Management, University of Washington, Seattle, WA 98195, USA; dannie70@uw.edu
[3] Department of Civil Engineering, First Technical University, Ibadan 23401, Nigeria; gideon.bamigboye@tech-u.edu.ng
* Correspondence: sjo0016@auburn.edu

Abstract

Reinforced concrete durability depends on a passive oxide film protecting embedded steel, sustained by high-alkalinity pore solutions. Cracking fundamentally alters transport, allowing rapid chloride and carbon dioxide ingress, which undermines passivity and accelerates corrosion. Self-healing concrete technologies aim to autonomously restore transport barriers and reestablish electrochemical stability. This review critically synthesizes evidence on healing effectiveness for corrosion mitigation through a dual framework of barrier restoration and interface stabilization, integrating depth-resolved chloride profiles with electrochemical performance indices. Critically, visual crack closure proves an unreliable indicator of corrosion protection. Healing mechanisms exhibit characteristic spatial signatures: autogenous and microbial approaches preferentially seal surface zones with diminishing effectiveness at reinforcement depth, while encapsulated low-viscosity polymers achieve greater depth continuity. However, electrochemical recovery consistently lags transport recovery, with healed specimens achieving only partial restoration of intact corrosion resistance. Recovery effectiveness depends on crack geometry, moisture conditions, and healing mechanism characteristics, with systems performing effectively only within narrow, condition-specific windows. Effective corrosion protection requires coordinated barrier and interface strategies targeting both bulk transport and steel surface chemistry. The path forward demands rigorous field validation emphasizing electrochemical outcomes over appearance metrics, long-term durability assessment, and performance-based verification frameworks to enable predictable service life extension.

Keywords: self-healing concrete; corrosion; reinforcement corrosion; chloride transport; Electrochemical Impedance Spectroscopy (EIS)

check for updates

Academic Editor: Ray Kai Leung Su

Received: 31 August 2025
Revised: 13 October 2025
Accepted: 23 October 2025
Published: 27 October 2025

Citation: Osibodu, S.J.; Akerele, D.D.; Bamigboye, G.O. Efficacy of Self-Healing Concrete for Mitigating Reinforcement Corrosion: A Critical Review of Transport Properties and Electrochemical Performance. *Buildings* **2025**, *15*, 3875. https://doi.org/10.3390/buildings15213875

Copyright: © 2025 by the authors. Licensee MDPI, Basel, Switzerland. This article is an open access article distributed under the terms and conditions of the Creative Commons Attribution (CC BY) license (https://creativecommons.org/licenses/by/4.0/).

1. Introduction

Reinforced concrete is fundamental to modern construction due to its high compressive strength, versatility, and inherent durability. However, its long-term performance depends on protecting the embedded steel reinforcement from corrosion, which causes infrastructure deterioration worldwide [1,2]. During cement hydration, the high alkalinity pore solution (pH about 12.5–13.8) promotes the formation of a protective passive oxide film on the

embedded steel surface, which is the primary defense against corrosion [3]. The passive film is often described as bi-layered, with Fe^{2+} oxides and oxyhydroxides near the steel and Fe^{3+} phases toward the pore solution, and a typical thickness of about 3 to 15 nm [4].

The vulnerability of this protective system becomes apparent when cracks develop in the concrete matrix. While dense, crack-free concrete cover delays aggressive ion ingress for decades, real-world structures invariably develop cracks from drying shrinkage, thermal gradients, settlement, or mechanical overload, creating preferential pathways for chlorides, carbon dioxide, moisture, and oxygen [5]. These transport pathways fundamentally alter the mass transfer regime from slow bulk matrix diffusion to rapid advection and capillary suction, dramatically shortening the corrosion initiation phase. The resulting electrochemical reactions produce expansive corrosion products that progressively reduce the rebar's cross-sectional area while inducing further cracking, spalling, and ultimately compromising structural safety [6–8].

Crack characteristics strongly influence corrosion rates, with critical widths often discussed around 0.1 to 0.5 mm, though consensus remains elusive because geometry, exposure, and concrete quality interact [9–11]. What is unequivocal is that unchecked cracking sharply accelerates corrosion initiation and propagation, threatening structural integrity and increasing lifecycle costs [12]. This fundamental vulnerability necessitates a paradigm shift from reactive repair strategies to proactive, intrinsic material resilience.

Self-healing concrete has emerged as a transformative technology designed to restore the protective barrier at the steel–concrete interface, thereby reestablishing passive conditions and blocking deleterious ion ingress [13,14]. The concept is based on incorporating components into the concrete matrix that can activate upon cracking to seal or heal the fissure. Self-healing mechanisms are broadly categorized as autogenous (leveraging intrinsic cementitious ability) and autonomous (involving engineered components such as encapsulation systems, biomineralization, and specialized admixtures) [15–20]. Additionally, emerging interface stabilization approaches, such as microbial-induced iron mineralization (MIIM), offer revolutionary potential for biochemical repassivation of corroded steel surfaces [21].

Despite extensive research demonstrating impressive crack closure in self-healing systems, a critical gap persists in the literature: a systematic evaluation of (i) transport restoration and (ii) long-term electrochemical protection to the reinforcement. Much of the existing literature focuses on the mechanics of healing and material formulation [12,22,23], with recent reviews summarizing quantitative data on reduced chloride penetration [16,24,25]. However, the fundamental issue is that visually healed cracks do not guarantee restored durability [16]. A crack that appears sealed may still offer a preferential pathway for chlorides and other aggressive agents, offering little improvement in corrosion protection. This highlights a critical 'healing-corrosion paradox' where physical repair does not translate to electrochemical stability. Therefore, the central question in the field has evolved from 'Can concrete heal a crack?' to 'How effectively does a healed crack restore barrier properties and prevent corrosion?' This distinction has profound implications for technology selection, service-life prediction [26], and the practical implementation of self-healing technologies in corrosive environments.

With aging infrastructure worldwide facing accelerating deterioration and multi-trillion-dollar replacement costs, self-healing concrete represents a potential paradigm shift from reactive repair to proactive resilience. However, deployment requires rigorous validation that healing effectiveness translates to genuine corrosion protection under realistic service conditions.

To address this knowledge gap, this review employs a dual-paradigm framework distinguishing between barrier restoration and interface stabilization to critically evaluate

self-healing effectiveness for corrosion protection. The analysis synthesizes evidence on how healing mechanisms restore transport properties and electrochemical stability, comparing effectiveness under varied exposures while identifying key factors governing real-world performance. The review proceeds from corrosion fundamentals and assessment metrics (Section 2), through technology overview (Section 3), to critical evaluation integrating depth-resolved transport with electrochemical performance and evidence-based selection guidance (Section 4), concluding with implementation perspectives and research priorities (Section 5).

2. Corrosion Mechanisms and Key Performance Metrics in Cracked Concrete

This section establishes the corrosion mechanisms and performance metrics that self-healing technologies must address, providing the analytical framework for evaluating barrier restoration and electrochemical stability in Section 4.

2.1. Corrosion Mechanism in Cracked Concrete

2.1.1. The Passive Film

The inherent corrosion resistance of reinforced concrete relies on a nanoscale passive oxide/hydroxide film (3–15 nm thick) composed of Fe^{2+} oxides/oxyhydroxides at the steel interface and Fe^{3+} phases toward the concrete. This film is formed and maintained by the high alkalinity of the concrete pore solution (pH about 12.5–13.8), which is rich in calcium, sodium, and potassium hydroxides [4,8]. This passive film, illustrated in Figure 1, acts as a highly effective barrier that reduces the rate of metal dissolution (corrosion) to a negligible level (typically <0.1 $\mu A/cm^2$), ensuring the long-term durability of the reinforcement [3]. However, this protection is vulnerable to environmental aggressors that penetrate through cracks (e.g., chloride and carbon dioxide), highlighting the need for self-healing to restore and maintain this passive state.

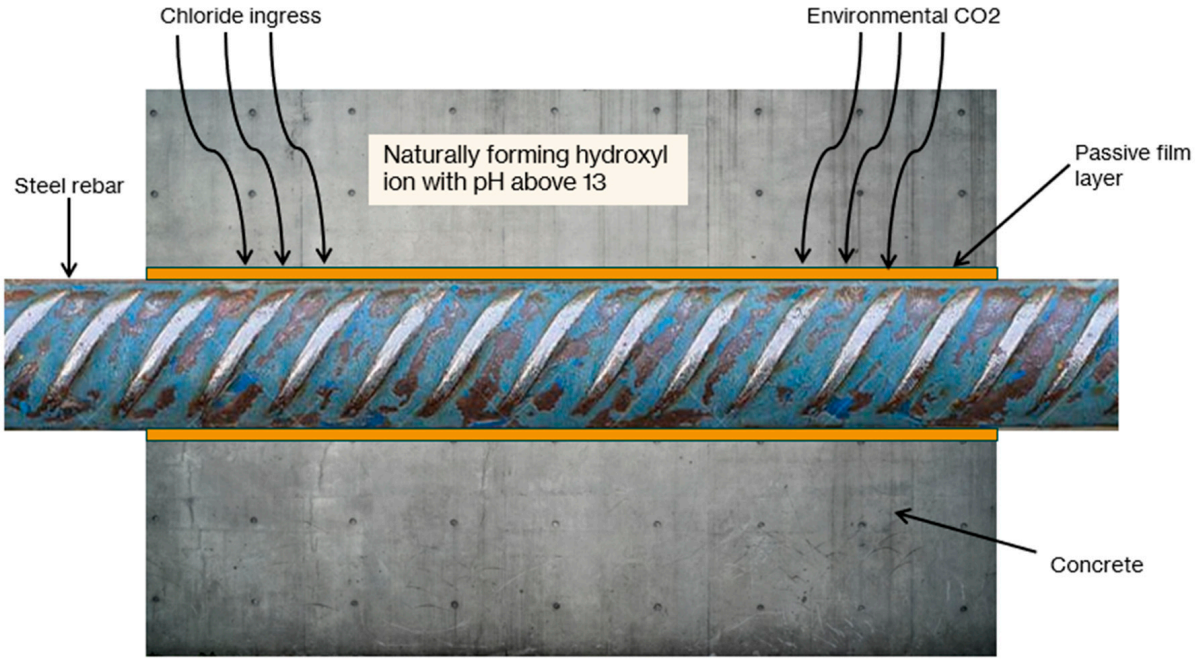

Figure 1. Conceptual illustration of the passive film layer in Reinforced Concrete.

2.1.2. Crack-Induced Transport and Depassivation

Cracks compromise the concrete cover's barrier function by creating preferential pathways that fundamentally alter the transport regime from slow, bulk matrix diffusion to rapid advection and capillary suction [11]. This shift bypasses diffusion through intact paste and shortens the initiation phase that normally dominates service life. The two primary depassivation mechanisms exacerbated by cracks are:

i. Chloride-Induced Corrosion: Chloride ions (Cl^-), typically from de-icing salts or marine environments, are particularly aggressive. When chlorides accumulate at the steel–concrete interface beyond a system-dependent critical threshold better expressed as the local $[Cl^-]/[OH^-]$ ratio rather than a single absolute chloride value, the passive film breaks down even at high pH [27,28]. This initiates a localized, autocatalytic pitting corrosion process that can cause significant loss of the rebar's cross-section with minimal visible warning on the concrete surface [29].
ii. Carbonation-Induced Corrosion: Atmospheric CO_2 reacts with alkaline phases, consuming the alkaline reserve and reducing pore solution pH. When carbonation reaches the reinforcement depth and pH drops to about 11 or below, the passive film stability is compromised, with complete depassivation typically observed around pH 9 to 10 [6,30]. Carbonation-induced corrosion is dependent on concrete resistivity, porosity and degree of saturation [3].

By facilitating rapid ingress of Cl^- and CO_2, cracks precipitate these mechanisms, necessitating self-healing strategies that seal pathways and reinstate chemical protection.

2.2. Key Metrics for Evaluating Corrosion Mitigation Efficacy

Rigorous evaluation of self-healing requires metrics that quantify barrier restoration and corrosion state. These are categorized into mass transport properties (assessing ingress resistance) and electrochemical indicators (directly measuring steel behavior), applied to cracked/healed specimens over time to capture healing dynamics.

2.2.1. Assessment of Mass Transport Properties (Barrier Performance)

These metrics evaluate how self-healing impedes aggressive agents, typically on controlled-crack specimens post-healing.

i. Chloride Ion Penetration: Critical for structures in marine or de-icing environments, chloride ion penetration is assessed through tests measuring chloride diffusion or migration coefficients. Chloride penetration is assessed via migration tests such as NT BUILD 492 or diffusion tests such as ASTM C1556, with lower coefficients indicating superior healing effectiveness.
ii. Carbonation Resistance: Evaluated by accelerated carbonation per BS EN 14630 [31], with shallower depths indicating enhanced protection.
iii. Water Permeability and Sorptivity: As water is a key electrolyte in corrosion, its ingress is a critical indicator. Permeability tests, for example, BS EN 12390-8 [32] measure water flow under pressure, while sorptivity tests such as ASTM C1585 [33] assess the rate of water absorption in unsaturated concrete. Significant reductions in these values after healing are vital for corrosion mitigation [34].
iv. Gas Permeability: Assessed using RILEM-CEMBUREAU methods, with lower permeability indicating improved barrier performance. Standardized moisture preconditioning is essential for meaningful comparison [35].
v. Electrical Resistivity: Measures concrete's ion flow resistance per ASTM C1876 [36], with higher resistivity indicating better corrosion protection.

Healing effectiveness is quantified by significant transport property reductions post-healing, reported as healed-to-cracked ratios or efficiency indices [37].

2.2.2. Assessment of Electrochemical Performance (Direct Corrosion State)

These metrics directly assess embedded steel electrochemical state:

i. Half-Cell Potential (HCP)/Open-Circuit Potential (OCP): Measured per ASTM C876 [38], potentials more negative than −0.35 V CSE indicate active corrosion, while values less negative than −0.20 V CSE indicate passivity. Healing effectiveness is confirmed by shifts toward less negative potentials.
ii. Corrosion Current Density (i_{corr}): Measured via Linear Polarization Resistance or Tafel polarization (ASTM G59). High polarization resistance (Rp) and low icorr (<0.1 $\mu A/cm^2$) indicate passive conditions, confirming healing efficacy.
iii. Electrochemical Impedance Spectroscopy (EIS): AC technique characterizing steel–concrete interface over 100 kHz to 1 mHz frequency range, depending on time stability [39]. Analysis using equivalent circuit models provides robust passive film integrity [40].

In addition, advanced localized methods (SVET, SECM) offer spatial corrosion current resolution but lack standardization for routine assessment [41]. Healing efficacy is indexed via shifts toward passive states: less negative HCP, lower icorr, higher Rp, or increased charge transfer resistance [42].

2.3. Key Takeaways

Cracks flip transport from slow diffusion to fast capillary and advection, collapsing the initiation window. Steel stays protected only while high pH sustains the passive film, and chloride risk is better judged by the local Cl^- to OH^- ratio than by any single threshold. Use transport tests to evaluate the barrier and electrochemical tests to evaluate actual steel protection. In practice, that means depth-resolved chloride or a validated surrogate plus time series HCP or OCP, Rp, icorr, Ecorr, and EIS. Always report crack width, geometry, moisture history, and conditioning because these govern comparability and achievable recovery.

3. Self-Healing Technologies and Their Relevance to Corrosion Inhibition

The development of self-healing concrete technologies can be categorized into a dual paradigm framework that differs fundamentally in their approach to corrosion mitigation: barrier restoration and interface stabilization [21,43]. The most common is "barrier restoration," where healing mechanisms physically seal cracks to block the transport of aggressive agents. A second, emerging mode is "interface stabilization," which aims to chemically or biochemically transform unstable corrosion products at the steel surface into a new, stable passive layer. Building on the mechanisms set out earlier, this section provides an integrated, critical reading of transport behavior (chloride ingress, sorptivity/permeability, resistivity) and electrochemical performance, with explicit applicability windows (crack width, exposure) and comparability caveats (mix design, crack induction, conditioning, exposure protocols).

This section draws upon comprehensive reviews in the field such as those by [14,37,43–45] to frame the current understanding. It also critically evaluates the principal autogenous and autonomous strategies, distinguishing between these approaches to analyze their underlying mechanisms, demonstrated performance, and inherent limitations as corrosion management solutions.

3.1. Barrier Restoration

The barrier restoration paradigm, the most common approach in self-healing concrete, encompasses mechanisms that primarily function by physically sealing cracks. This preventative strategy aims to block transport pathways for aggressive agents like chlorides and CO_2, thereby extending the corrosion initiation phase. However, the effectiveness of these methods are critically dependent on the quality, stability, and chemical compatibility of the healing products formed.

3.1.1. Autogenous Healing: Intrinsic Sealing Mechanism

Autogenous healing relies on intrinsic material properties, primarily continued hydration of unreacted cement particles and the precipitation of calcium carbonate ($CaCO_3$) from the carbonation of calcium hydroxide [13,46]. However, its corrosion mitigation efficacy is limited by incomplete barrier restoration and compromised chemical stability. While these mechanisms can reduce crack connectivity and limit ingress of aggressive agents, their efficacy in mitigating reinforcement corrosion is highly contingent on the restoration of transport barriers and electrochemical stability. Carbonation-driven $CaCO_3$ precipitation reduces the local alkaline reserve and narrows the passivity margin governed by the local Cl^- to OH^- balance, so passive stability is typically compromised as pH drops toward about 11 or below [4,47]. In reinforced systems, this poses a risk of depassivation, especially if the carbonation front reaches the steel–concrete interface [27,47]. For autogenous healing, ongoing hydration is more pronounced at early ages under sustained moisture, and $CaCO_3$ precipitation is seen more during wet–dry cycles indicating the longer time required for acceptable healing [48,49].

Consequently, improved watertightness does not assure restored passivity or that the healed region will resist chloride-ion penetration like the uncracked section [50]. This matches experimental observations where autogenous healing often shows strong reductions in water flux for tight cracks but only partial and slower recovery in chloride transport [48]. Water permeability serves as the most sensitive quantitative index for self-healing assessment, with sealing-ratio metrics effectively capturing early recovery stages [34]. By contrast, measurements of chloride transport through cracked/healed specimens report reductions rather than full restoration relative to uncracked controls, with outcomes strongly governed by crack width, wet–dry preconditioning, and curing regime [49,51,52]. Consistent with these dependencies, controlled studies and syntheses indicate that autogenous healing effectively stabilizes chloride ingress only for very tight cracks ($\leq$0.10–0.15 mm) [50,53]. Beyond this range, improvements diminish rapidly without auxiliary measures [48].

Two coupled trade-offs generally limit autogenous healing as a corrosion-mitigation tool. First, in samples with higher supplementary cementitious materials (SCMs), pozzolanic/latent-hydraulic reactions consume portlandite [$Ca(OH)_2$], which lowers readily available Ca^{2+} and OH^- for fast $CaCO_3$ precipitation. While SCMs can sustain later-age hydration and refine pores, controlled studies and syntheses show reduced early crack-healing efficiency as SCM content increases unless ample moisture is supplied [43,46,54]. Second, when carbonation-driven products dominate the fill, closure often proceeds near the surface via $CaCO_3$ formation from CH (and, at higher extents, from decalcifying C–S–H), but this consumes the alkaline reserve and lowers pH into ranges incompatible with robust steel passivity; hence, "closure" may coincide with reduced electrochemical safety margin at the interface [27,47,55]. Together, these effects explain why autogenous healing can delay corrosion initiation relative to an open crack yet often fails to fully restore the transport barrier or interfacial chemistry of intact cover in chloride-bearing exposures, which is the healing corrosion paradox that closure does not equal passivity [16,43,48].

Autogenous healing is most effective for microcracks ≤0.10–0.15 mm in elements with a reliable moisture supply, which sustains continued hydration while keeping the carbonation front away from the steel depth. Suitable contexts are elements with sustained moisture availability and tight crack control, consistent with evidence that autogenous healing is most effective under immersion or wet–dry exposure [56,57]. In practice, this often aligns with interior/underground environments with high relative humidity and water-retaining structures where crack widths are controlled. In keeping with laboratory evidence under immersion or wet–dry regimes, autogenous closure can supplement transport resistance where external chloride load is low and crack widths are tightly controlled [6,8]. Caution is warranted in marine splash and deicing environments, freeze–thaw regimes, combined carbonation–chloride exposures, aggressive chemical environments, or poor crack-width control (≥0.15–0.20 mm), where closure does not ensure passivity [10,55,58]. Given the limited long-term electrochemical evidence for autogenous healing under realistic cycling, relying on it alone for long design lives in aggressive exposures is not recommended [16,43].

Autogenous healing is particularly advantageous because it provides intrinsic, moisture-activated sealing with watertightness gains for tight microcracks, high matrix compatibility, and synergy with auxiliaries such as SAPs in the microcrack regime [56,57,59–61]. Moreover, this mechanism is inherent to the material, requiring no engineered additives, making it a cost-effective solution for sealing fine cracks (typically <0.2 mm). Its efficacy is limited by several factors. First, the healing potential diminishes over time as unhydrated cement is consumed. Second, carbonation-induced healing, while physically sealing a crack, consumes the alkaline reserve (portlandite), which can lower the local pH at the steel–concrete interface. This creates a central trade-off of autogenous healing: the process of physical repair can inadvertently make the electrochemical environment more conducive to corrosion. As a result, while it can reduce water permeability, its ability to restore resistance to chloride ingress is often incomplete and variable [43,47,48,54].

Recent numerical modeling reinforces these depth-dependent limitations. Wang et al. [62] demonstrated through damage–healing–transport coupling that tensile displacements below 5 μm have minimal transport impact. However, beyond this threshold chloride migration accelerates dramatically with a 66% concentration increase at 15 mm depth with 10 mm displacement. Their 100-year simulations showed that even healing rates of 70–90% leave chloride content at 30 mm depth at 35–75% of unhealed levels, confirming that autogenous healing's protective window narrows sharply with crack size and depth.

3.1.2. Autonomous Healing via Engineered Solutions

To overcome the limitations of autogenous healing, particularly for wider cracks (>0.2 mm), autonomous healing strategies incorporate engineered components designed to deliver a more robust and reliable repair.

a. Microbial-Induced Calcite Precipitation (MICP) for Barrier Restoration

Non-pathogenic, spore-forming bacteria (e.g., Bacillus genus) are incorporated into concrete with nutrients. Water ingress into a crack revives the dormant bacteria, which metabolize the nutrients (e.g., through ureolysis) to precipitate a dense plug of calcium carbonate ($CaCO_3$), sealing the crack [63,64]. MICP has demonstrated the ability to seal cracks up to 1.0 mm wide, significantly outperforming autogenous healing. The process can create a dense, crystalline barrier against water and chloride ingress. Nonetheless, critical challenges to its long-term viability in real-world structures persist. The potential for ammonium by-products from the urea cycle remains a concern, although management strategies are being developed. Finally, the long-term stability and erosion resistance of the precipitated calcite compared to the cement matrix, especially under acidic or flowing conditions, is not yet fully established [21,65,66].

In concrete, the dominant pathway is ureolysis, where urease hydrolyzes urea to ammonium and carbonate; at high pH, carbonate combines with Ca^{2+} to nucleate calcite and sometimes aragonite on crack walls, progressively forming a mineral plug that reduces hydraulic connectivity [67,68]. Across controlled studies, MICP delivers reliable crack closure and substantial permeability reductions under immersion or wet–dry regimes for moderate crack widths, with routine, reproducible healing around about 0.3 to 0.5 mm, and larger apertures occasionally achieved in optimized laboratory protocols that combine adequate agent supply, favorable geometry, and sustained moisture [12,69,70]. With respect to chloride transport, improvements are frequently observed but rarely match uncracked references. Depth-resolved observations show that $CaCO_3$ often concentrates near the crack mouth and within shallow zones of the cover, so surface closure does not necessarily translate into deep zone transport suppression [25,71]. Consistent with this, electrochemical improvements are seen only when the fill is continuous and adherent and local chemistry at the steel interface remains favorable; hence, the persistent closure does not equal passivity caveat for barrier-centric strategies [25,66].

A central constraint on long-term effectiveness is microbial survivability in concrete: high alkalinity (pH = 12.5–13.8), hydration heat, desiccation, and oxygen/moisture availability govern activity windows and repeatability; survivability improves with protective carriers and co-culture strategies, but multi-decade durability data remain scarce [12,66]. Ureolysis also produces ammonium, which requires management, and two-stage treatments such as rinsing coupled with struvite recovery can capture NH_4^+ but add process complexity [72]. From a materials perspective, $CaCO_3$ fills can be vulnerable in acidic/abrasive exposures, and geometry/moisture remain first-order levers [69,70].

Filamentous fungi such as *Rhizopus oryzae*, *Trichoderma longibrachiatum*, *Aspergillus* spp. can likewise precipitate $CaCO_3$ via alkalization/ureolysis and promote organomineralization on chitin-rich hyphae, providing abundant nucleation templates and a physical scaffold for dense precipitate formation [73,74]. Compatibility is strain-specific and conditioned by pH, moisture, and surface/pore characteristics [75,76]. Given the sensitivity of fungal growth/mineralization to the concrete micro-environment and the limited long-horizon electrochemical datasets in reinforced systems, there is a need to validate durability and electrochemical responses in reinforced systems before generalizing fungal benefits from small-scale matrices.

For both bacteria and fungi, the primary functional gain is transport-side. Watertightness improves rapidly for micro- to meso-scale cracks as calcite bridges nucleate and densify, with demonstrated reductions in water absorption/permeability and moderated chloride transmission [70,71,77].

Simulated marine exposure reveals critical performance limitations. In a particularly revealing study, Youssa Tchamou and Xue [78] investigated Bacillus subtilis-treated reinforced concrete exposed to seawater and found that bacterial specimens exhibited no crack healing, chloride concentrations 78–123% higher than controls after 84 days, and systematically decreasing linear polarization resistance indicating accelerating corrosion rates over 98 days. The bacterial precipitation paradoxically increased matrix porosity, facilitating rather than preventing chloride ingress, a stark demonstration that surface mineralization does not ensure deep-zone corrosion protection in aggressive marine environments

However, three durability caveats temper corrosion-mitigation claims. First, survivability is the principal rate-limiting factor; many spores/cells are damaged during cure or starved in service, leading to spatially heterogeneous mineralization and incomplete sealing at depth [63,66,73]. Second, the calcite phase can be susceptible to dissolution under acidic or cyclic wetting environments; fungal and bacterial plugs may erode faster than the C-S-H matrix under certain chemistries, necessitating exposure-aware design [74–76].

Third, even strong transport improvements do not automatically guarantee electrochemical passivity at steel in chloride-bearing exposures; data linking microbial healing to long-term half-cell potential, polarization resistance, or EIS stability in reinforced systems remain sparse relative to transport studies and must be expanded under realistic cycling [66,78]. Accordingly, MICP should be positioned as a barrier-restoration strategy, often highly effective for liquid tightness, whose corrosion benefits depend on crack geometry, depth of sealing, exposure chemistry, and persistence of the precipitate.

From an application standpoint, MICP is best suited to members with a reliable moisture supply and controllable, moderate crack widths around 0.3–0.5 mm, where a mineral plug compatible with the cement matrix is desirable. Where deep zone chloride resistance is critical or acidic or abrasive exposures are credible, MICP should not be relied on as a stand-alone corrosion control measure. Cost and scale-up remain practical hurdles, though fungal culture and handling may be simpler than bacterial in some supply chains [73,77].

MICP is advantageous due to autonomous activation with moisture, large water-tightness gains for micro- to meso-cracks, and in fungal systems, rich nucleation scaffolds that can accelerate dense carbonate growth; immobilization significantly enhances viability and fill efficiency [70,71,73,74,77]. Limitations include survivability in high alkalinity, by-product management for ureolysis, exposure sensitivity of carbonate phases, a relatively narrow practical crack width window without carriers, and incomplete evidence that transport recovery alone ensures long horizon passivity in chloride-prone environments [63,72,75,79].

b. Chemical-Induced Self-Healing

Chemical self-healing restores the transport barrier via predictable reactions between an introduced healing chemistry and the cracked cementitious matrix (or pore solution/CO_2), producing C-S-H gels, insoluble crystals, expansive hydrates, or polymerized solids that occlude cracks. Unlike microbial routes, activation depends on moisture, alkalinity, or temperature rather than cell viability. Representative families include crystalline admixtures (CAs), reactive mineral salts including sodium silicate, calcium nitrate, CSA, or MgO, and in-situ polymerizing systems such as DCPD/ROMP; polyurethane and epoxy [80–83]. Table 1 summarizes these system types, their core reaction, compatibility notes, and caveats.

Table 1. Chemical-Induced Self-Healing Systems [80–87].

System Type	Core Reaction & Product	Environmental/Compatibility Notes	Key Caveats
Crystalline admixtures (CAs)	Moisture-activated reaction with hydration by-products → insoluble crystalline networks that block pores/cracks; co-growth with late hydration	Moisture-dependent; synergy with fibers/expansive agents; good matrix compatibility	Depth of sealing can be limited without sustained moisture; chloride resistance at depth may be partial

Table 1. *Cont.*

System Type	Core Reaction & Product	Environmental/Compatibility Notes	Key Caveats
Sodium silicate	Silicate + $Ca(OH)_2$ → secondary C-S-H/C-A-S-H gel densify crack flanks and adjacent paste	Watch gel syneresis/shrinkage under drying; potential local CH depletion at high dose	Depth-limited without delivery aid; composition/curing sensitive
Calcium nitrate (CN)	Predominantly Ca^{2+} supply → promotion of crack-filling hydrates/$CaCO_3$; redox schematics in literature are heuristic in alkaline pore solution	Mechanism narratives vary; capsule shell chemistry can affect strength	Consider mechanical trade-offs at high dosage; verify depth of seal
CSA/MgO/CaO (expansive)	Hydration/expansion → AFt/AFm/CH/brucite; stress-assisted closure + mineral fill	Risk of over-expansion; exposure stability of ettringite	Geometry/curing sensitive; monitor for secondary cracking
Polymers (PU/epoxy/DCPD-ROMP)	Polymer networks form in-crack (ROMP/cross-linking; moisture-curing urethane/urea)	Interface durability governs life; thermal mismatch/shrinkage to watch	Viscosity–depth trade-off; vet leachates/aging

3.2. Interface Stabilization

In fundamental contrast to the barrier restoration paradigm, which focuses on the physical blocking of transport pathways, the 'interface stabilization' paradigm targets the electrochemical root of the corrosion process itself. The core idea of this paradigm is active electrochemical intervention rather than passive physical blocking. These technologies are not primarily designed to seal the bulk of a crack; instead, they aim to biochemically or chemically modify the steel–concrete interface to restore or enhance the protective passive film [11,21,88].

3.2.1. Microbial-Induced Iron Mineralization (MIIM) for Interface Stabilization

MIIM addresses corrosion at its source by stabilizing the steel–concrete interface rather than closing cracks. Iron-reducing bacteria respire Fe(III) within rust phases such as lepidocrocite and goethite to Fe(II) and, in the presence of suitable anions, precipitate compact ferrous minerals, principally siderite ($FeCO_3$) and vivianite ($Fe_3(PO_4)_2 \cdot 8H_2O$), directly on the steel surface. These adherent low-permeability layers suppress anodic dissolution and help maintain a passive-like state, positioning MIIM as an interface stabilization route that complements barrier restoration [21,88,89].

Under low oxygen conditions with an available electron donor such as lactate, acetate, or hydrogen, organisms including *Shewanella oneidensis* reduce Fe(III) oxides through dissimilatory pathways mediated by extracellular electron transfer proteins such as the MtrCAB complex [90,91]. The interfacial redox step is:

$$Fe^{3+} + e^- \rightarrow Fe^{2+}$$

Representative donor oxidation is illustrated by lactate:

$$C_3H_5O_3^- + 2\,H_2O \rightarrow C_2H_3O_2^- + HCO_3^- + 4\,H^+ + 4\,e^-$$

Accumulated Fe^{2+} then precipitates ferrous minerals when carbonate or phosphate activity at the interface is sufficient:

$$Fe^{2+} + CO_3{}^{2-} \rightarrow FeCO_3(s)$$

$$3\,Fe^{2+} + 2\,PO_4{}^{3-} + 8\,H_2O \rightarrow Fe_3(PO_4)_2{\cdot}8H_2O(s)$$

Film identity and texture are governed by local redox potential, pH, and anion availability. Because bulk concrete pore solution is highly alkaline, MIIM generally relies on micro-niche engineering at the steel rust interface using biofilms, encapsulants, hydrogels, and rust porosity to keep dissolved oxygen low, present donors and anions, and maintain favorable chemistry long enough for continuous Fe(II) layers to assemble [21,88].

Laboratory studies demonstrate that iron-reducing communities can generate continuous Fe phosphate layers that cover more than ninety percent of corroded iron surfaces. Film continuity is critical since discrete islands offer limited protection, whereas dense adherent layers stabilize the corrosion stratigraphy and lower corrosion activity relative to untreated controls [21]. The magnitude of corrosion rate reduction depends on system chemistry, exposure, and the continuity of the ferrous mineral film. Performance should be reported alongside film coverage and composition rather than inferred from visual presence alone [21,88].

Successful implementation requires precise control of several parameters. Oxygen must remain below critical thresholds to preserve anaerobic conditions, electron donors must be available to sustain metabolism, and carbonate or phosphate must exceed supersaturation limits for mineral growth [88]. MIIM offers direct electrochemical repassivation potential through dense Fe(II) mineral formation and may self-repair under continued microbial activity, representing an environmentally oriented approach that converts existing rust into protective phases [88,92]. Constraints include the narrow environmental window for bacterial viability, the challenge of sustaining activity in alkaline concrete over long durations, and the need for delivery and monitoring strategies that maintain the required micro niche at steel depth [89]. MIIM is best suited to contexts with reliable moisture and controllable oxygen ingress, such as interior elements, soil contact members, or rehabilitation with direct steel access, and it should be paired with barrier restoration because it does not provide crack closure [21].

3.2.2. Chemical Interface Stabilization

Chemical interface stabilization acts directly at the steel–concrete interface to (re)establish passivity through adsorption films from organics and oxide chemistry modification from inorganics, rather than by physically sealing cracks in the cover. Three families dominate: (i) molecular adsorption barriers, for example, amines and amino alcohols, (ii) migrating corrosion inhibitors (MCIs) formulated to reach embedded steel, and (iii) inorganic anodic inhibitors such as nitrite and molybdate that rebuild the passive film via controlled redox and film growth pathways [93–95].

a. Molecular adsorption barriers (organics): Amines and amino alcohols protect by chemisorption of the polar headgroup on iron sites with outward packing of hydrophobic chains, forming dense molecular films that restrict water, oxygen, and chloride and slow interfacial charge transfer. In reinforced-concrete contexts, migrating amino-alcohol formulations and internally dosed amines reduce corrosion when sufficient inhibitor reaches the steel, with efficacy modulated by cover permeability and moisture regime [93,96]. Mechanistic analogues on steel support the renewable-film concept, but translation to reinforced concrete requires validated delivery to rebar and confirmation of interfacial coverage in alkaline pore solution [95].

b. Migrating corrosion inhibitors: MCIs are designed to migrate through the pore network and adsorb on embedded steel as mixed inhibitors. Bridge scale and laboratory rehabilitation studies on chloride-contaminated concrete reported more noble potentials and reduced corrosion indices when MCIs were combined with appropriate repairs and coatings, provided transport to steel was feasible [96]. Conversely, controlled mortar tests under active pitting observed high diffusion of the volatile amine component yet no measurable rate reduction, implicating insufficient delivery of the non-volatile fraction to the steel surface [93]. Thus, MCIs are delivery-limited.

c. Inorganic anodic repassivation: Nitrite (NO_2^-) supports anodic repassivation by oxidizing Fe^{2+} at active sites and fostering Fe(III) oxide/oxyhydroxide growth (e.g., γ-FeOOH, Fe_2O_3). Representative steps are often summarized as:

$$2Fe^{2+} + 2OH^- + 2NO_2{}^- \rightarrow 2NO + Fe_2O_3 + H_2O$$

$$Fe^{2+} + OH^- + NO_2{}^- \rightarrow NO + \gamma - FeOOH$$

Efficacy scales with the molar ratio $n(NO_2^-)/n(Cl^-)$ is typically observed for $\gtrsim$ 1.0–1.2 in chloride-only exposure, with higher demand as pH decreases [94,97]. Molybdate ($MoO_4{}^{2-}$) functions as an oxyanion modifier that competes with Cl^- and can be incorporated into Fe-oxide structures, thickening the passive layer in alkaline media; responses are context-dependent, so dose, pH, and co-ion conditions must be validated in concrete-like environments [98,99].

Across organics and inorganics, a common success condition emerges: adequate inhibitor activity at the steel surface. Practically, this requires: (i) deliverability (migration or triggered release) through the cover, (ii) exposure support (moisture/temperature) to permit transport and sustain interfacial reactions, and (iii) threshold-aware dosing, especially for nitrite where the molar ratio must exceed critical values and for organics where surface coverage governs film integrity [93–96].

In relation to traditional cathodic protection (CP), CP is an externally powered electrochemical intervention that shifts potential to suppress anodic dissolution; it does not depend on forming a specific interfacial film [27]. By contrast, chemical interface stabilization is dose and delivery-limited interfacial chemistry. In new construction, practical routes include integral nitrite dosing where chloride risk is credible, ensuring that the nitrite to chloride ratio at steel depth remains above threshold over time, and embedded delivery of organics via microcapsules positioned near reinforcement. In rehabilitation, MCIs and nitrite injections or surface treatments can stabilize the interface when transport to steel is achievable [93,96]. CP remains the most robust option when assured control is paramount, whereas chemical stabilization is advantageous where power-free, chemistry-based passivation can be delivered and verified under the intended exposure [27,94]. Table 2 summarizes the Self-Healing Techniques covered in this review.

Table 2. Comparative Summary of Self-Healing Techniques for Corrosion Mitigation [12,21,83,87,100,101].

Paradigm	Healing Technique	Primary Mechanism	Key Advantages	Limitations/Disadvantages	Reported Performance Metrics
Barrier Restoration	Autogenous Healing	Continued hydration of unreacted cement and carbonation of $Ca(OH)_2$.	- Inherent to concrete; no additional cost. - Effective for sealing very fine cracks.	- Healing potential diminishes with concrete age. - Carbonation consumes alkalinity (risk of pH drop). - Limited to sealing, not structural repair.	- Crack Width: Effective up to ~0.1–0.15 mm (wetting required). - Chloride Reduction: Surface closure > depth recovery;
	Autonomous: Encapsulation (Polymers)	Rupture of capsules releases liquid polymers (e.g., polyurethane) that polymerize in the crack.	- Heals wider cracks effectively. - Delivers a large volume of robust, adhesive healing agent. - Low-viscosity agents offer deep crack penetration.	- High material cost and complex manufacturing. - Risk of capsule damage during mixing. - Long-term stability/bond of polymer-concrete interface is a concern.	- Crack Width: Up to 0.3 mm and wider. - Chloride Reduction: Up to 36% at 15 mm depth (low-viscosity PU)
	Autonomous: Microbial-Induced Calcite Precipitation (MICP)	Bacteria (e.g., Bacillus species) metabolize nutrients upon water ingress, precipitating $CaCO_3$ as a crack sealant.	- Biocompatible and potentially sustainable. - Can seal relatively wide cracks with a dense precipitate	- Long-term viability of bacteria in high-pH concrete is uncertain. - Potential for harmful by-products (e.g., ammonia from urea cycle). - Stability of precipitated calcite vs. cement matrix.	- Crack Width: routinely ~0.3–0.5 mm; up to ~1.0 mm reported under optimized conditions. - Chloride Reduction: reductions are stronger near the surface and taper with depth without tailored delivery or extended cycling. 12–15% at mid-depth zones.
	Autonomous: Superabsorbent Polymers (SAP)	SAPs absorb water, swelling to physically block the crack, while also releasing stored water to fuel autogenous healing	- Dual-action: physical blockage and internal curing agent. - Can repeatedly swell and shrink.	- Can create large voids if not properly designed. - Potential negative impact on initial mechanical strength. - High cost.	- Can improve water tightness significantly for cracks < 0.3 mm. Chloride reduction: gains are less consistent than watertightness and depend on mix/SAP dosing

Table 2. *Cont.*

Paradigm	Healing Technique	Primary Mechanism	Key Advantages	Limitations/Disadvantages	Reported Performance Metrics
	Autonomous: Crystalline Admixtures (CA)	Proprietary chemicals react with moisture and cement by-products to form insoluble, pore-blocking crystalline structures.	- Becomes a permanent, integral part of the concrete. - Can activate years after placement upon water ingress. - No complex encapsulation required.	- Mechanisms are proprietary and less transparent. - Effectiveness is highly dependent on crack width and water availability.	- Crack Width: Effective up to 0.4 mm reported.
Interface Stabilization	Microbial-Induced Iron Mineralization (MIIM)	Iron-reducing bacteria biochemically transform unstable rust (Fe^{3+}) into a dense, stable, and passivating biogenic mineral layer (e.g., $FeCO_3$).	- Directly addresses the electrochemical root of corrosion. - Transforms a porous rust layer into a protective barrier.	- Technology is in a nascent stage. - Requires specific (hypoxic/anaerobic) environmental conditions. - Relies on availability of electron donors.	- Performance data is emerging; focuses on electrochemical stability (e.g., increased R_p) rather than crack sealing.
	Chemical Inhibitors (Migrating/Encapsulated)	Molecules adsorb onto the steel surface, forming a protective film that inhibits anodic or cathodic reactions.	- Directly interferes with the corrosion process. - Encapsulation allows for targeted release upon cracking. - Effectiveness depends on concentration at steel (risk of under-dosing).	- Migrating inhibitors are limited by concrete transport properties	- Performance measured by electrochemical indicators (lower icorr, higher R_p).
		Anodic inhibitors (e.g., NO_2^-, MoO_4^{2-}) compete with Cl^- to chemically stabilize and reform the passive oxide film on the steel.	- Directly restores the protective passive layer. - Proven effectiveness in high-chloride environments	- Requires a critical inhibitor-to-chloride ratio to be effective; ineffective or even detrimental if underdosed. - Potential for leaching.	- Performance: Depends on maintaining $[NO_2^-]/[Cl^-]$ ratio > 1.2.

3.3. Delivery System

The efficacy of any healing mechanism depends on putting the right agent in the right place at the right time. Carrier strategies used in concrete, including microcapsules, hollow or sacrificial fibers, and vascular networks, rely on crack-triggered release to place sufficient inventory within the fracture plane [102–104]. Encapsulation is attractive because it delivers a targeted dose and can extend repair beyond the micro-crack regime, provided the core rheology favors penetration and the cured fill maintains a durable bond to the surrounding paste [87,105]. However, outcomes are fundamentally delivery-limited: dispersion must be uniform, rupture thresholds must prevent premature breakage during mixing while ensuring activation under service cracking, and the healed interface must not evolve into a future ion pathway as it ages [102,106]. Practical incorporation therefore emphasizes mixing energy and sequence control to preserve carrier integrity while retaining crack-time responsiveness [106]. Microencapsulation challenges for phase change materials in concrete, where capsule survivability, shell integrity, and leakage prevention similarly govern effectiveness, demonstrate that these constraints represent fundamental materials engineering challenges requiring standardized protocols [107]. Within the dual paradigm framework, barrier restoration requires depth-reaching release for reinforcement-level chloride control, whereas interface stabilization demands steel-proximal positioning for threshold concentrations at the steel–concrete interface. Verification must include depth-resolved transport, time-series electrochemistry, and mechanism-specific checks. Comprehensive reviews are available elsewhere [104–106].

3.4. Key Takeaways

Two levers address two failure modes. Barrier restoration and interface stabilization work best when designed together. Autogenous healing helps to seal tight microcracks in wet service, microbial and crystalline routes tend to seal near the crack mouth, while encapsulated low viscosity polymers are the most reliable for depth continuity. Interface routes such as nitrite, amino alcohols, and MIIM can reestablish passivity even with partial closure, but they are delivery and threshold-limited. Carriers, viscosity, trigger, and dose govern outcomes, so design delivery around the protection target and plan to verify it.

4. Discussion and Critical Evaluation

Self-healing concrete presents a fundamental paradox: technologies that demonstrably reduce chloride transport often fail to prevent reinforcement corrosion. This disconnect reveals deeper problems in how healing effectiveness is evaluated and applied, rooted in three critical failures: measurement artifact confusion, depth-dependent healing incompleteness, and electrochemical hysteresis that resists reversal. The measurement challenge begins at the most basic level. As Angst et al. [28] demonstrated, the "critical chloride content" threshold, a metric many studies use to claim success, is not a fixed material property but an artifact of measurement timing and definition, leading to reported values scattered over two orders of magnitude. This ambiguity is critical when evaluating real-world performance, where delayed detection of corrosion is often mistaken for enhanced protection. The fundamental issue is that corrosion risk depends on the local Cl^-/OH^- ratio at the steel surface rather than any single threshold concentration. This distinction becomes critical when evaluating healing systems that alter local pore chemistry.

This paradox is starkly illustrated by the conflicting performance of Microbial-Induced Carbonate Precipitation (MICP) systems. While earlier studies by Jonkers et al. [63], Luo et al. [69], and Ling and Qian [71] demonstrated protective effects under periodic or wet–dry exposure conditions, more recent research by Youssa Tchamou and Xue [78] revealed that it failed under continuous seawater immersion. Specifically, their study

documented substantially elevated chloride concentrations (72% higher for 4% bacterial content), significant compressive strength drops (49–51%), and continuously decreasing linear polarization resistance over 98 days, concluding "MICP-concrete samples immersed in seawater and sodium chloride solutions showed no healing capability." Corroborating these findings, recent reviews by Sukumaran et al. [108] and Pooja and Tarannum [109] confirm this exposure-regime dependency as a persistent challenge across bacterial systems, noting that healing mechanisms effective under cyclic wetting can paradoxically become vulnerabilities under static immersion, possibly by increasing porosity or creating preferential pathways through incompletely mineralized zones. The following sections deconstruct this paradox by examining two distinct failure patterns and exploring an alternative paradigm that targets the steel–concrete interface.

4.1. Transport Performance and the Depth Discontinuity Challenge

The first pattern is the depth discontinuity challenge, where systems successfully reduce chloride ingress near the crack surface but show limited effectiveness at depths approaching the reinforcement. This spatial heterogeneity fundamentally undermines the assumption that surface-level measurements predict deep-zone protection.

Figure 2 illustrates this fundamental relationship, showing how crack closure kinetics vary dramatically with initial crack width under continuous immersion conditions. The data reveal that, while narrow cracks (≤0.1 mm) can achieve greater than 80% closure within weeks, wider cracks plateau at incomplete closure, establishing the physical basis for why surface healing does not guarantee deep-zone protection.

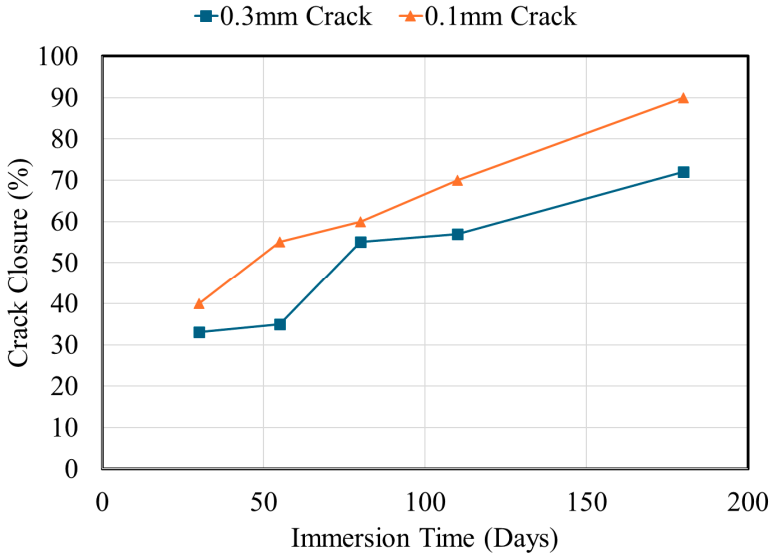

Figure 2. Crack closure kinetics as a function of immersion time for different initial crack widths in OPC mortar specimens. Data from [48].

This incomplete closure translates directly to depth-dependent transport performance. Capelleso et al. [110] documented this clearly in crystalline admixture (CA) concrete, where healing is robust in narrow cracks (0.1 mm) but incomplete in wider ones (0.3 mm), with healing products like ettringite and aragonite concentrated in the outer regions. This creates a vulnerable deep zone where chlorides accumulate, leading to localized concentration spikes precisely where they cause maximum damage. Figure 3 shows bacterial healing achieves 8-15% chloride reduction across all depths, while autogenous healing increases surface chloride content by 18% despite visual crack closure.

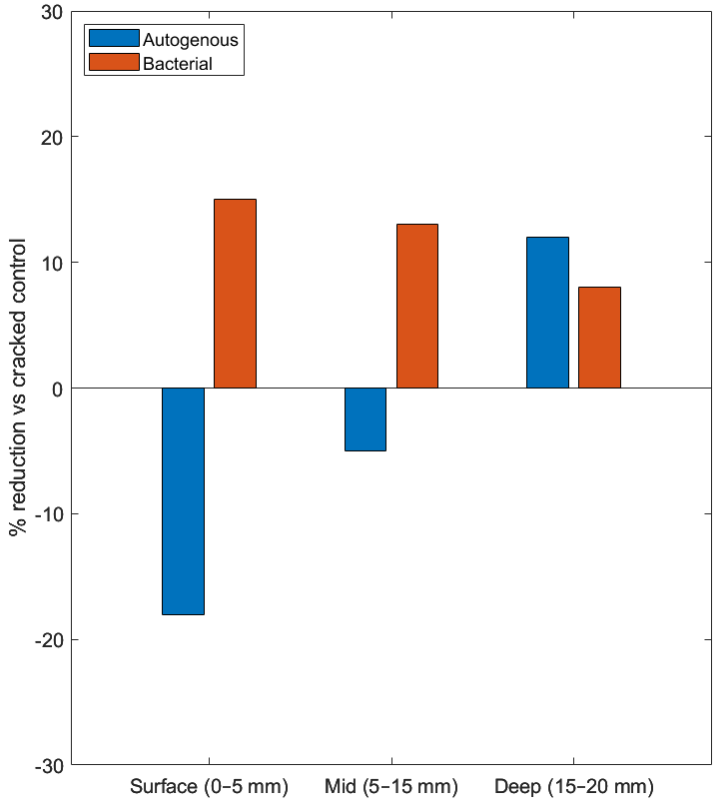

Figure 3. Depth-resolved reduction in chloride ingress relative to cracked controls for autogenous and bacterial healing in OPC mortar/concrete [71]. Results are expressed as percentage reduction in chloride content compared to cracked reference specimens, binned into surface (0–5 mm), mid (5–15 mm), and deep (15–20 mm) zones. Negative values indicate higher chloride content.

Chloride concentrations at reinforcement depth can actually exceed those in unhealed cracks despite apparent surface sealing. Park and Choi [52] formalized this with their residual crack width concept, acknowledging that healing is rarely complete and the unsealed portion governs transport at depth. Tumeinne et al. [20] recently emphasized this limitation in their comprehensive review, noting that while autonomous systems like encapsulated polymers and MICP can address wider cracks (>0.3–0.5 mm), the challenge of ensuring complete and uniform healing at depth remains a significant barrier to widespread adoption. The viscosity of the healing agent is a critical factor. Van Belleghem et al. [87] showed that low-viscosity PU achieves better deep penetration and maintains low macro-cell corrosion currents (<3 μA) and high anodic polarization resistance (28–40 kΩ), comparable to uncracked specimens. In contrast, high-viscosity PU creates a surface cap that fails to protect the steel, with macro-cell currents persisting above 20 μA and polarization resistance collapsing to <3.5 kΩ, indicating active corrosion comparable to untreated cracked specimens. Figure 4 demonstrates this viscosity-depth relationship: low-viscosity formulations achieve 30–40% chloride reductions that increase with depth, while high-viscosity PU worsens due to shallow capping rather than depth penetration.

This is an important revelation; the distribution of the healing product, not its total volume, determines effectiveness. This pattern extends to bacterial systems, where even with measurable $CaCO_3$ deposition, corrosion occurred at reduced rates, suggesting incomplete sealing at depth, even when surface examination suggested good healing [71]. Several factors contribute to depth-dependent healing effectiveness, including healing agent viscosity, crack width, and exposure conditions (e.g., wet–dry cycling vs. continuous immersion). Biological constraints, such as oxygen availability, can also limit bacterial activity in deeper crack zones, a limitation recently confirmed by [109] in their review of bacterial viability

challenges in concrete. No current bacterial healing technology consistently overcomes the depth discontinuity challenge for cracks wider than 0.1 to 0.15 mm in realistic exposure conditions, representing a fundamental limitation of transport-focused healing approaches.

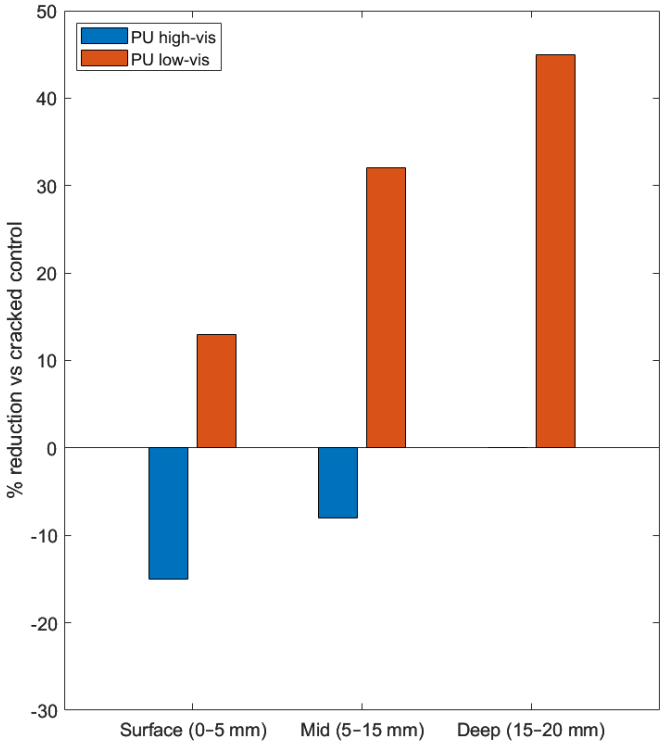

Figure 4. Depth-resolved reduction in chloride ingress relative to cracked controls for polyurethane (PU) injection systems in cracked concrete [87]. Results are expressed as percentage reduction in chloride content compared to cracked reference specimens, binned into surface (0–5 mm), mid (5–15 mm), and deep (15–20 mm) zones. Negative values indicate higher chloride content.

Having established that transport recovery alone proves insufficient, attention must now turn to the second fundamental failure pattern: the persistent gap between achieved and desired electrochemical performance.

4.2. Electrochemical Performance and the Partial Recovery Ceiling

The second pattern is the partial recovery ceiling, where systems achieve significant but incomplete restoration of corrosion resistance, reaching a performance limit well below that of uncracked concrete regardless of apparent healing quality. This is rooted in electrochemical hysteresis: once depassivation occurs (typically when local Cl^-/OH^- ratios exceed critical thresholds [28] or pH drops below approximately 11–11.5 [6,47]), repassivation requires more stringent conditions than the original passive state [27,47].

Table 3 summarizes representative electrochemical trajectories from key self-healing studies organized by healing mechanism. Each entry documents three performance stages: baseline values for uncracked concrete, post-crack values indicating initial damage state, and post-healing values showing recovered performance after specified healing duration.

Table 3. Summary of Electrochemical Performance Metrics from Representative Self-Healing Studies.

Healing Mechanism	Concrete Type [Crack Width, mm]	Exposure Condition	Uncracked Baseline	Post-Crack Peak Damage	Post-Healing State	Healing Duration	Key Findings
Polyurethane capsules (HV) [a] [87]	OPC, w/b = 0.41, FA = 15% [0.30]	Weekly wet–dry; 33 g/L NaCl	Imacro ≈ 0 μA; Ecorr −50 to +100 mV vs. SCE [b]; Rp,A [c] > 20 kΩ	Imacro 40–51 μA (week 1); ΔE [d] 260–430 mV; Rp,A 4–8.5 kΩ	Imacro remained > 20 μA; ΔE > 430 mV; Rp,A < 3.5 kΩ at 26 weeks	26 weeks	High-viscosity formulation failed to penetrate crack depth; electrochemical behavior equivalent to unhealed cracked specimens
Polyurethane capsules (LV) [a] [87]	OPC, w/b = 0.41, FA = 15% [0.30]	Weekly wet–dry; 33 g/L NaCl	Imacro ≈ 0 μA; Ecorr −50 to +100 mV vs. SCE; Rp,A > 20 kΩ	Imacro 40–51 μA (week 1); ΔE 260–430 mV; Rp,A 4–8.5 kΩ	From week 14: Imacro < 3 μA; Rp,A 28–40 kΩ; ΔE 150–200 mV at 26 weeks	26 weeks	Low-viscosity formulation achieved deep penetration; electrochemical parameters approached but did not fully restore uncracked values
Phytate + molybdate inhibitor coating [e] [111]	Mortar [artificial scratch]	3.5% NaCl	Rp ≈ 2200 kΩ·cm^2; Ecorr ≈ −180 mV vs. SCE	— [f]	Rp ≈ 800–1200 kΩ·cm^2; Ecorr ≈ −260 mV	140 days	Interface stabilization slowed Rp degradation; potentials remained well above active corrosion threshold
Control coating (no inhibitor) [111]	Mortar [artificial scratch]	3.5% NaCl	Rp ≈ 2200 kΩ·cm^2; Ecorr ≈ −180 mV vs. SCE	— [f]	Rp ≈ 350–450 kΩ·cm^2; Ecorr ≈ −350 to −380 mV	140 days	Without interface stabilization, potentials crossed into active corrosion range; severe Rp collapse
Bacteria-based self-healing (BAS) [110]	OPC, w/c = 0.50 [0.10 and 0.30]	Artificial seawater (marine)	— [f]	— [f]	For 0.30 mm cracks: Ecorr indicated "high" corrosion probability after 60–70 days; For 0.10 mm cracks: initiation evidence at 58–74 days	12 months	Despite reduced chloride ingress, potentials indicated passivity breakdown in cracked specimens; performance better for narrower cracks
Crystalline admixture (CA) [110]	OPC, w/c = 0.50 [0.10 and 0.30]	Artificial seawater (marine)	— [f]	— [f]	For 0.10 mm healed cracks: Ecorr remained above −200 mV (low corrosion probability) throughout exposure	12 months	Stronger coupling between transport recovery and electrochemical stability than BAS; limited effectiveness for 0.30 mm cracks

Footnotes: [a] HV = high viscosity; LV = low viscosity; [b] SCE = saturated calomel electrode reference (standard electrochemical reference electrode); [c] Rp,A = area-normalized anodic polarization resistance (kΩ); resistance of steel to corrosion measured in anodic regions. Higher values indicate better corrosion resistance.; [d] ΔE = driving potential (mV); potential difference between anodic (corroding) and cathodic (protected) regions. Higher values indicate stronger corrosion driving force. [e] Interface stabilization approach (coating applied to rebar surface) rather than barrier restoration through crack sealing; [f]—indicates parameter not measured or not reported in original study. Symbol definitions: Imacro = macro-cell corrosion current (μA) between damaged and undamaged concrete regions; values <0.1 μA/cm^2 indicate passive steel; Ecorr = corrosion potential (mV vs. SCE); values >−200 mV indicates passive conditions; values <−350 mV indicate active corrosion; intermediate values (−200 to −350 mV) suggest uncertain or transitional states; Rp = polarization resistance (kΩ·cm^2); measure of steel's resistance to electrochemical dissolution; higher values indicate lower corrosion rates.

Quantitative analysis of the data in Table 3 reveals this ceiling. For interface stabilization approaches, Liu et al. [111] demonstrated that phytate–molybdate coatings achieved only 36–55% restoration of polarization resistance (800–1200 kΩ·cm^2 versus 2200 kΩ·cm^2 for uncracked mortar) after 140 days in 3.5% NaCl solution, with corrosion potentials stabilizing at intermediate values (−260 mV vs. SCE) more noble than open cracks (typically <−350 mV vs. SCE indicating active corrosion per ASTM C876 [38]) but more negative than passive steel (>−200 mV vs. SCE [38]). Similarly, Ma et al. [112] documented this ceiling in a dual-responsive microcapsule system, where the best-performing formulation achieved only 55.62% restoration of charge transfer resistance, leaving the specimen at roughly half the corrosion resistance of intact controls. Qian et al. [113] showed that a combined microbial repair and protective film system provided synergistic but still incomplete protection, not reaching the performance of uncracked specimens.

This suggests that crack healing addresses one corrosion driver (bulk chloride transport through cracks) but not others, such as the steel surface condition. Van Belleghem et al.'s [87] study reveals the complexity of defining recovery. Their low-viscosity polyurethane system achieved anodic polarization resistance (28–40 kΩ) approaching or exceeding uncracked baseline values (>20 kΩ) and reduced driving potentials (150–200 mV versus 260–430 mV at peak damage), suggesting substantial electrochemical recovery. However, macro-cell corrosion current never reached the sub-microampere levels (<0.1 μA) typical of truly passive steel, remaining above 3 μA even after 26 weeks. Critically, concrete resistance recovered to uncracked-similar levels, indicating successful bulk property restoration, but anodic polarization resistance, which directly reflects steel surface electrochemistry, remained distinguishable from uncracked controls in terms of corrosion current density. This decoupling demonstrates that different electrochemical metrics recover at different rates and to different extents, with interfacial processes lagging bulk transport restoration. The ceiling effect becomes more pronounced with extended exposure. Notably, Youssa Tchamou and Xue [78] tracked linear polarization resistance (LPR) in bacterial concrete over 98 days in seawater, showing continuous decrease and eventually corrosion rates exceeding unhealed controls, suggesting that healing products themselves became part of the corrosion problem. For bacterial systems in marine environments, Cappellesso et al. [110] observed that both bacteria-based and crystalline admixture specimens showed evidence of corrosion initiation within 58–74 days despite reduced chloride ingress, with potentials indicating passivity breakdown even for narrow (0.10 mm) cracks. Only crystalline admixture specimens with 0.10 mm healed cracks and maintained potentials above −200 mV (low corrosion probability) throughout the 12-month exposure [110].

Several mechanisms contribute to the recovery ceiling. First, healing products rarely achieve the same pore structure as virgin concrete, creating different ionic transport properties or susceptibility to chloride attack [110]. Second, the steel–concrete interface may be permanently altered once corrosion initiates, leaving nanoscale damage that healing cannot fully reverse. Third, and perhaps most concerning, healing products may introduce new electrochemical vulnerabilities, such as localized alkalinity reduction from soluble sodium carbonate precipitates, which can destabilize the passive film [3,110,114].

4.3. Interface Stabilization: An Alternative Paradigm

Given the inherent limitations of purely barrier-restoring mechanisms documented above, interface stabilization emerges as a more direct and robust paradigm. This approach aims to chemically or biochemically modify the steel surface to provide electrochemical protection, even if crack sealing is incomplete. In essence, this strategy directly addresses the healing corrosion paradox by shifting the focus from physical crack repair to direct electrochemical intervention at the steel–concrete interface, thereby offering a more direct route to maintaining passivity. Bio-electrochemical approaches exemplify this. Nitrate-reducing, carbonate-precipitating consortia simultaneously generate passivating nitrite and sealing carbonates at the steel interface [115]. Microbially induced iron mineralization converts rust to adherent, protective ferrous mineral films (vivianite, siderite, or magnetite) directly on steel, suppressing anodic dissolution [21]. The key distinction from MICP crack filling is location: interface-localized mineral films remain effective even when crack regions distant from reinforcement receive incomplete healing. Similarly, biofilm-based protection [116] and biomimetic hydroxyapatite conversion coatings [117] have shown success by forming protective layers directly on the steel. This paradigm shift from bulk repair to targeted interfacial protection offers a more promising path to durable corrosion resistance.

4.4. Selection Framework

An evidence-based selection framework must account for these patterns to guide practitioners toward appropriate technology choices. The following synthesis integrates the failure patterns identified above with demonstrated performance windows to provide actionable guidance. The choice of a self-healing strategy depends on the specific application, expected crack widths, and exposure conditions. Data consistently converge on crack width as the primary determinant of healing effectiveness. Starting with the narrowest cracks, for cracks below 0.1 mm, crystalline admixtures have demonstrated effective prevention with wet–dry cycling [52,110]. Moving to the intermediate range, for cracks between 0.1–0.3 mm, low-viscosity encapsulated systems as developed by Van Belleghem et al. [87] provide a demonstrated option. However, for cracks exceeding 0.3 mm, conventional healing consistently fails. Systems that perform well under wet–dry cycling often fail under continuous immersion. For splash zones (wet–dry conditions), bacterial and CA systems are viable for cracks below 0.1 mm. For tidal or submerged zones, only encapsulated polymers have shown protection, limited to a maximum crack width of 0.1–0.15 mm. Reliable assessment necessitates electrochemical monitoring during exposure to detect depassivation. The available evidence, limited to exposure durations of 12 months or less [87,110], is insufficient to determine whether healing proportionally extends service life or merely delays corrosion initiation by a fixed period. The partial recovery ceiling mandates modeling healed concrete as a distinct material condition with intermediate corrosion resistance. Several critical uncertainties currently prevent the confident deployment of self-healing concrete for corrosion mitigation, including healing product durability, performance under repeated damage, scale effects, temperature effects, and economic viability. The current framework is therefore provisional. Systems demonstrating laboratory promise require field validation under controlled conditions before deployment in critical infrastructure.

4.5. Key Takeaways

The evidence synthesized above converges on three critical principles that must guide both research priorities and practical implementation:

First, closure does not equal passivity. Visual crack sealing correlates poorly with electrochemical protection due to two consistent failure patterns: depth discontinuity, where surface improvements mask incomplete reinforcement-depth sealing, creating localized chloride spikes; and partial recovery ceiling, where healed specimens plateau at 40–60% of intact corrosion resistance regardless of transport improvements.

Second, performance windows are narrow and condition-dependent. Autogenous and bacterial systems seal cracks below 0.1 mm under wet–dry cycling but fail under continuous immersion. Low-viscosity encapsulated polymers extend this to 0.2 mm but never fully restore passivity. Beyond 0.3 to 0.5 mm, conventional healing fails. As an alternative, interface stabilization (MIIM, inhibitor coatings) offers alternative protection targeting steel surface chemistry, though it requires pairing with barrier methods and remains delivery-limited.

Third, effective evaluation demands depth-resolved chloride profiling paired with time-series electrochemical monitoring under realistic exposure. Critically, current evidence limited to 12-month horizons captures less than 2% of target service life. Therefore, confident deployment for critical infrastructure requires multi-year field validation demonstrating that healing extends service life by predictable, economically justifiable periods under actual service conditions.

5. Conclusions and Future Perspectives

This review critically evaluated self-healing concrete technologies for reinforcement corrosion mitigation through a dual-paradigm framework: restoring transport barriers along crack paths and stabilizing the steel–concrete interface. Through systematic analysis of transport and electrochemical evidence, this review establishes that visual crack closure, a frequently reported metric, provides an unreliable indication of corrosion protection. Fundamentally, closure alone does not ensure passivity unless healing products achieve depth continuity to the reinforcement and the interface chemistry supports sustained passivation. The local chloride-to-hydroxide ratio and pH at the steel surface, rather than a single bulk threshold concentration, more reliably determine corrosion risk.

The synthesis of available evidence yields three key conclusions that define the current state of knowledge:

1. Crack geometry and exposure regime fundamentally dictate the achievable ceiling of recovery. Healing effectiveness declines sharply beyond narrow crack widths for autogenous systems and moderate widths for encapsulated approaches. Continuous immersion critically undermines systems effective under wet–dry cycling.
2. Healing mechanisms exhibit characteristic spatial signatures. Autogenous and microbial approaches preferentially seal surface zones with depth-dependent attenuation. In contrast, low-viscosity encapsulated polymers can achieve greater depth continuity, while chemical or biological interface modifiers aim to secure passivity independently of bulk crack closure.
3. Electrochemical recovery consistently lags transport recovery. Healed specimens typically achieve only partial restoration of intact corrosion resistance, with corrosion potentials stabilizing at intermediate values. Single-mechanism approaches, by addressing only one failure mode, prove insufficient under aggressive exposure conditions.

5.1. Technology-Specific Applicability Windows

Based on these findings, specific applicability windows for current self-healing technologies can be delineated as follows:

1. Autogenous healing is effective for microcracks under sustained moisture. However, while it improves watertightness, it only partially restores chloride resistance at depth. Furthermore, carbonation-driven precipitation consumes the alkaline reserve, lowering pH and narrowing the passivity margin. Consequently, autogenous healing should not be solely relied upon in aggressive environments such as marine splash zones, deicing applications, combined carbonation–chloride exposure, or freeze–thaw conditions.
2. Microbial-induced calcite precipitation reliably seals moderate cracks under wet–dry cycling. However, mineral deposition concentrates near crack mouths, and continuous seawater immersion can lead to catastrophic failure, characterized by elevated chloride levels and accelerating corrosion. MICP systems therefore require fundamental redesign for continuously submerged marine applications or should be excluded from such environments.
3. Encapsulated low-viscosity polymers demonstrate superior penetration to reinforcement depth and exhibit the strongest coupling between chloride reduction and electrochemical protection. High-viscosity formulations primarily seal surfaces but fail at depth, underscoring the critical importance of viscosity selection. These systems are suitable for moderate cracks in chloride-rich environments.

4. Crystalline admixtures effectively prevent corrosion for narrow cracks during marine exposure under wet–dry cycling. However, performance degrades for wider cracks and continuous immersion.
5. Chemical interface stabilization shifts protection from transport-dependent to threshold-dependent mechanisms. Nitrite, for example, requires a critical molar ratio to chloride at the steel depth, with higher demand as pH decreases. Phytate–molybdate coatings and similar systems maintain passivity despite coating damage by establishing protective layers directly on steel.
6. Microbial-induced iron mineralization converts rust to adherent ferrous mineral films directly on steel, thereby suppressing anodic dissolution. This approach is promising in environments where oxygen can be controlled, and moisture is reliable. MIIM must be paired with barrier methods, as it provides interface stabilization without crack closure.

5.2. Evidence-Based Verification Standards

Selection and verification protocols must be performance-based rather than appearance-based to circumvent the disconnect between crack closure and passivity documented throughout this review. A minimum verification framework should include the following four complementary assessment categories:

1. Transport Assessment: This requires depth-resolved chloride profiling from the surface to the reinforcement, not merely surface measurements. Validated migration or diffusion surrogates under standardized preconditioning are essential. Verification must confirm that chloride concentrations at reinforcement depth remain below critical thresholds.
2. Electrochemical Monitoring: Time-series tracking during exposure is necessary to detect depassivation as it occurs. Confirmation that potentials remain in passive ranges is crucial; values indicating active corrosion or transitional states must be identified. Verification that polarization resistance approaches intact specimen values, not just improvement over cracked controls, is also vital. A target corrosion current density characteristic of passive steel should be aimed for.
3. Mechanism-Specific Verification: This involves assessing polymer penetration depth and continuity via microscopy. Local inhibitor ratios at steel depth can be determined via pore solution analysis. Film continuity for interface stabilization approaches should be assessed via surface analysis, and mineral plug density and adhesion for microbial systems via microstructural characterization.
4. Standardized Reporting: Mandatory disclosure of crack width distribution, concrete composition, cover depth, detailed exposure regime, and moisture history is essential to enable cross-study comparison and meta-analysis.

When these diagnostic criteria align, healing demonstrably achieves both transport barrier restoration at depth and passivity security at the steel interface.

5.3. Future Research Priorities

To advance the field, several critical research priorities emerge that address the knowledge gaps identified above:

1. Multi-cycle damage-healing protocols: Simulate multiple crack–heal–recrack cycles from thermal, mechanical, and continued degradation. Track electrochemical performance through each cycle to determine whether healing agent reservoirs deplete and whether accumulated steel interface damage creates progressive vulnerability. This will critically distinguish systems that extend service life cumulatively from those that merely redistribute corrosion risk temporally.

2. Integrated barrier-plus-interface systems: Test combined approaches hypothesized to address both failure patterns, such as encapsulated polymers with admixed inhibitors, microbial precipitation with triggered inhibitor release, or crystalline admixtures with interface stabilization additives. The key question is whether predicted synergies materialize under the full verification suite outlined in Section 5.2.
3. Delivery verification protocols: Transition from bulk dosing assumptions to steel-surface measurement. Develop standardized methods quantifying inhibitor concentration, biogenic film coverage, and mineral continuity at the steel–concrete interface. This directly addresses the consistent finding that interface approaches often fail due to delivery constraints rather than mechanism inadequacy.
4. Healing product stability characterization: Track the composition and electrochemical function of healing products over multi-year periods under service conditions. Quantify the dissolution kinetics of soluble phases. Determine whether healing products maintain favorable local pH and chloride-to-hydroxide ratios at steel depth or evolve into long-term vulnerabilities. Correlate chemical changes with electrochemical transitions from passive to active states.
5. Electrochemical threshold definition: Establish minimum polarization resistance values, potential ranges, and chloride-to-hydroxide ratios required to extend service life by specific periods under defined exposures. This will enable the transition from qualitative claims to quantitative service life prediction and provide design values for performance-based specification.
6. Economic validation and lifecycle comparison: Compare the total costs of self-healing concrete against conventional protection using actual service life data from field validation. Account for uncertainty penalties associated with intermediate corrosion states, which require more frequent inspection than virgin concrete. This will establish economic viability thresholds.
7. Biological system environmental robustness: Develop extremophile strains or protective encapsulation maintaining local microenvironments suitable for bacterial activity under temperature extremes, pH variations, and desiccation–rewetting cycles. Quantify mineral plug erosion under freeze–thaw, abrasion, and acidic exposure. Resolve catastrophic failure modes observed under continuous marine immersion through fundamental mechanism redesign or exclusion from submerged applications.

Author Contributions: Conceptualization, S.J.O., D.D.A. and G.O.B.; validation, S.J.O., D.D.A. and G.O.B.; data curation, S.J.O.; writing—original draft preparation, S.J.O. and D.D.A.; writing—review and editing, S.J.O., D.D.A. and G.O.B. All authors have read and agreed to the published version of the manuscript.

Funding: This research received no external funding.

Data Availability Statement: No new data were created or analyzed in this study.

Conflicts of Interest: The authors declare no conflicts of interest.

References

1. Ali, M.; Shams, M.A.; Bheel, N.; Almaliki, A.H.; Mahmoud, A.S.; Dodo, Y.A.; Benjeddou, O. A Review on Chloride Induced Corrosion in Reinforced Concrete Structures: Lab and in Situ Investigation. *RSC Adv.* **2024**, *14*, 37252–37271. [CrossRef]
2. He, S.; Sayadi, S.; Patel, R.A.; Schultheiß, A.L.; Mihai, I.C.; Jefferson, A.; Jonkers, H.M.; Luković, M.; Schlangen, E.; Dehn, F. Perspectives on the Incorporation of Self-healing in the Design Practice of Reinforced Concrete Structures. *Struct. Concr.* 2025; *Online ahead of print*. [CrossRef]
3. Ming, J.; Wu, M.; Shi, J. Passive Film Modification by Concrete Carbonation: Re-Visiting a Corrosion-Resistant Steel with Cr and Mo. *Cem. Concr. Compos.* **2021**, *123*, 104178. [CrossRef]

4. Williamson, J.; Isgor, O.B. The Effect of Simulated Concrete Pore Solution Composition and Chlorides on the Electronic Properties of Passive Films on Carbon Steel Rebar. *Corros. Sci.* **2016**, *106*, 82–95. [CrossRef]
5. Chemrouk, M. The Deteriorations of Reinforced Concrete and the Option of High Performances Reinforced Concrete. *Procedia Eng.* **2015**, *125*, 713–724. [CrossRef]
6. Zhou, Y.; Gencturk, B.; Willam, K.; Attar, A. Carbonation-Induced and Chloride-Induced Corrosion in Reinforced Concrete Structures. *J. Mater. Civ. Eng.* **2015**, *27*, 04014245. [CrossRef]
7. Bhuvaneshwari, B.; Selvaraj, A.; Iyer, N.R. Corrosion Inhibitors for Increasing the Service Life of Structures. In *New Materials in Civil Engineering*; Elsevier: Amsterdam, The Netherlands, 2020; pp. 657–676. [CrossRef]
8. Folić, R.; Zenunović, D.; Brujić, Z. Effects of Carbonation and Chloride Ingress on the Durability of Concrete Structures: Scientific Paper. *J. Serb. Chem. Soc.* **2024**, *89*, 729–742. [CrossRef]
9. Shaikh, F.U.A. Effect of Cracking on Corrosion of Steel in Concrete. *Int. J. Concr. Struct. Mater.* **2018**, *12*, 3. [CrossRef]
10. Basteskår, M.; Engen, M.; Kanstad, T.; Fosså, K.T. A Review of Literature and Code Requirements for the Crack Width Limitations for Design of Concrete Structures in Serviceability Limit States. *Struct. Concr.* **2019**, *20*, 678–688. [CrossRef]
11. Kanavaris, F.; Coelho, M.; Ferreira, N.; Azenha, M.; Andrade, C. A Review on the Effects of Cracking and Crack Width on Corrosion of Reinforcement in Concrete. *Struct. Concr.* **2023**, *24*, 7272–7294. [CrossRef]
12. Omoregie, A.I.; Wong, C.S.; Rajasekar, A.; Ling, J.H.; Laiche, A.B.; Basri, H.F.; Sivakumar, G.; Ouahbi, T. Bio-Based Solutions for Concrete Infrastructure: A Review of Microbial-Induced Carbonate Precipitation in Crack Healing. *Buildings* **2025**, *15*, 1052. [CrossRef]
13. Rumman, R.; Bediwy, A.; Alam, M.S. Revolutionizing Concrete Durability: Case Studies on Encapsulation-Based Chemical (Autonomous) Self-Healing Techniques and Future Directions—A Critical Review. *Case Stud. Constr. Mater.* **2024**, *20*, e03216. [CrossRef]
14. De Belie, N.; Gruyaert, E.; Al-Tabbaa, A.; Antonaci, P.; Baera, C.; Bajare, D.; Darquennes, A.; Davies, R.; Ferrara, L.; Jefferson, T.; et al. A Review of Self-Healing Concrete for Damage Management of Structures. *Adv. Mater. Interfaces* **2018**, *5*, 1800074. [CrossRef]
15. Kanellopoulos, A.; Giannaros, P.; Al-Tabbaa, A. The Effect of Varying Volume Fraction of Microcapsules on Fresh, Mechanical and Self-Healing Properties of Mortars. *Constr. Build. Mater.* **2016**, *122*, 577–593. [CrossRef]
16. Meraz, M.M.; Mim, N.J.; Mehedi, M.T.; Bhattacharya, B.; Aftab, M.R.; Billah, M.M.; Meraz, M.M. Self-Healing Concrete: Fabrication, Advancement, and Effectiveness for Long-Term Integrity of Concrete Infrastructures. *Alex. Eng. J.* **2023**, *73*, 665–694. [CrossRef]
17. Eisa, A.M.; Tahwia, A.M.; Osman, Y.A.; Elemam, W.E. Characteristics of Bacteria Based Self Healing Rubberized Concrete for Sustainable and Durable Construction. *Sci. Rep.* **2025**, *15*, 14758. [CrossRef]
18. Wang, J.; Wu, M. A Preliminary Study on an Effective and Simplistic Self-Healing Concept for Cement Using Coarse Clinker Particles as the Healing Agent. *Cem. Concr. Res.* **2025**, *193*, 107859. [CrossRef]
19. Galano, S.; Calabrese, A.; Asvapathanagul, P.; Shadravan, S.; Ly, M.; Flores, D.; Hernandez, M.; Rahmani, M. Innovative Approaches to Enhancing Concrete Compressive Strength: An Extensive Investigation of Biochar-Embedded and Self-Repairing Techniques. *J. Mater. Civ. Eng.* **2025**, *37*, 04025112. [CrossRef]
20. Tumwiine, H.; Chala, T.; Ssenyonjo, H.; Kirigoola, D.; Al-Fakih, A. On the Use of Self-Healing Materials in Concrete Technology: A Comprehensive Review of Materials, Mechanisms, and Field Applications. *Mater. Today Chem.* **2025**, *48*, 103001. [CrossRef]
21. Namakiaraghi, P.; Verdú, I.; Rahmaninezhad, A.; Musfirah, S.; Hubler, M.H.; Najafi, A.R.; Sales, C.M.; Farnam, Y.A. Microbial-Induced Stable Iron Mineral Production for Corrosion Mitigation Application in Reinforced Concrete. *Cem. Concr. Compos.* **2025**, *163*, 106214. [CrossRef]
22. Sidiq, A.; Gravina, R.; Giustozzi, F. Is Concrete Healing Really Efficient? A Review. *Constr. Build. Mater.* **2019**, *205*, 257–273. [CrossRef]
23. Raza, M.N.; Hussain, S.; Singh, M.; Yadav, J.S. A Review and Bibliometric Study of Bacteria-Based Self-Healing of Concrete. *Multiscale Multidiscip. Model. Exp. Des.* **2024**, *7*, 1–14. [CrossRef]
24. Venkatesh, C.; Mohiddin, S.K.; Ruben, N. Corrosion Inhibitors Behaviour on Reinforced Concrete—A Review. In *Sustainable Construction and Building Materials*; Das, B.B., Neithalath, N., Eds.; Springer: Singapore, 2019; pp. 127–134.
25. Zhu, H.; Hu, Z.; He, K.; Yang, H.; Kong, D.; Pan, R. Chloride Transport and Intelligent Repair Processes in Microencapsulated Self-Healing Concrete: A Review. *J. Build. Eng.* **2024**, *98*, 110988. [CrossRef]
26. Liu, Q. Progress and Research Challenges in Concrete Durability: Ionic Transport, Electrochemical Rehabilitation and Service Life Prediction. *RILEM Tech. Lett.* **2022**, *7*, 98–111. [CrossRef]
27. Bertolini, L.; Elsener, B.; Pedeferri, P.; Redaelli, E.; Polder, R.B. *Corrosion of Steel in Concrete: Prevention, Diagnosis, Repair*; John Wiley & Sons: Hoboken, NJ, USA, 2013; ISBN 978-3-527-65171-9.
28. Angst, U.; Elsener, B.; Larsen, C.K.; Vennesland, Ø. Critical Chloride Content in Reinforced Concrete—A Review. *Cem. Concr. Res.* **2009**, *39*, 1122–1138. [CrossRef]

29. Taheri-Shakib, J.; Al-Mayah, A. Effect of Corrosion Pit Distribution of Rebar on Pore, and Crack Characteristics in Concrete. *Cem. Concr. Compos.* **2024**, *148*, 105476. [CrossRef]
30. Das, B.B.; Singh, D.N.; Pandey, S.P. Rapid Chloride Ion Permeability of OPC- and PPC-Based Carbonated Concrete. *J. Mater. Civ. Eng.* **2012**, *24*, 606–611. [CrossRef]
31. *BS EN 14630*; Products and Systems for the Protection and Repair of Concrete Structures. Test Methods. Determination of Carbonation Depth in Hardened Concrete by the Phenolphthalein Method. BSI Group: London, UK, 2006.
32. *BS EN 12390-8*; Testing Hardened Concrete—Depth of Penetration of Water under Pressure. BSI Group: London, UK, 2019.
33. *ASTM C1585*; Standard Test Method for Measurement of Rate of Absorption of Water by Hydraulic-Cement Concretes. ASTM International: West Conshohocken, PA, USA, 2020.
34. Hou, S.; Li, K.; Wu, Z.; Li, F.; Shi, C. Quantitative Evaluation on Self-Healing Capacity of Cracked Concrete by Water Permeability Test—A Review. *Cem. Concr. Compos.* **2022**, *127*, 104404. [CrossRef]
35. Zhang, D.; Li, K. Concrete Gas Permeability from Different Methods: Correlation Analysis. *Cem. Concr. Compos.* **2019**, *104*, 103379. [CrossRef]
36. *ASTM C1876*; Standard Test Method for Bulk Electrical Resistivity or Bulk Conductivity of Concrete. ASTM International: West Conshohocken, PA, USA, 2024.
37. De Belie, N.; Van Belleghem, B.; Erşan, Y.Ç.; Van Tittelboom, K. Durability of Self-Healing Concrete. *MATEC Web Conf.* **2019**, *289*, 01003. [CrossRef]
38. *ASTM C876*; Standard Test Method for Corrosion Potentials of Uncoated Reinforcing Steel in Concrete. ASTM International: West Conshohocken, PA, USA, 2022.
39. Figueira, R.B. Electrochemical sensors for monitoring the corrosion conditions of reinforced concrete structures: A review. *Appl. Sci.* **2017**, *7*, 1157. [CrossRef]
40. Huang, A.; Chen, Q.; Xie, L.; Zhang, Q.; Sun, Y.; Li, B.; Li, W.; Jiang, Z.; Zhu, H. EIS Based Assessment of Electrodeposition Effect of Concrete Cracks: Experiment and Equivalent Model. *Constr. Build. Mater.* **2023**, *377*, 131080. [CrossRef]
41. Gonzalez-Garcia, Y.; Garcia, S.J.; Mol, J.M.C. Electrochemical Techniques for the Study of Self Healing Coatings. In *Active Protective Coatings: New-Generation Coatings for Metals*; Hughes, A.E., Mol, J.M.C., Zheludkevich, M.L., Buchheit, R.G., Eds.; Springer: Dordrecht, The Netherlands, 2016; pp. 203–240. ISBN 978-94-017-7540-3.
42. *ASTM G59*; Standard Test Method for Conducting Potentiodynamic Polarization Resistance Measurements. ASTM International: West Conshohocken, PA, USA, 2023.
43. Cappellesso, V.; di Summa, D.; Pourhaji, P.; Prabhu Kannikachalam, N.; Dabral, K.; Ferrara, L.; Cruz Alonso, M.; Camacho, E.; Gruyaert, E.; De Belie, N. A Review of the Efficiency of Self-Healing Concrete Technologies for Durable and Sustainable Concrete under Realistic Conditions. *Int. Mater. Rev.* **2023**, *68*, 556–603. [CrossRef]
44. Das, R.; Gandhi, I.S.R.; Palanisamy, M. A Critical Review on Properties of PCM-Incorporated Cementitious Building Materials. *Adv. Civ. Eng. Mater.* **2023**, *12*, 271–294. [CrossRef]
45. Amran, M.; Onaizi, A.M.; Fediuk, R.; Vatin, N.I.; Muhammad Rashid, R.S.; Abdelgader, H.; Ozbakkaloglu, T. Self-Healing Concrete as a Prospective Construction Material: A Review. *Materials* **2022**, *15*, 3214. [CrossRef]
46. De Rooij, M.; Van Tittelboom, K.; De Belie, N.; Schlangen, E. (Eds.) *Self-Healing Phenomena in Cement-Based Materials: State-of-the-Art Report of RILEM Technical Committee 221-SHC: Self-Healing Phenomena in Cement-Based Materials*; RILEM State-of-the-Art Reports; Springer: Dordrecht, The Netherlands, 2013; Volume 11, ISBN 978-94-007-6623-5.
47. Huet, B.; L'Hostis, V.; Miserque, F.; Idrissi, H. Electrochemical Behavior of Mild Steel in Concrete: Influence of pH and Carbonate Content of Concrete Pore Solution. *Electrochim. Acta* **2005**, *51*, 172–180. [CrossRef]
48. Maes, M.; Snoeck, D.; De Belie, N. Chloride Penetration in Cracked Mortar and the Influence of Autogenous Crack Healing. *Constr. Build. Mater.* **2016**, *115*, 114–124. [CrossRef]
49. Luo, M.; Jing, K.; Bai, J.; Ding, Z.; Yang, D.; Huang, H.; Gong, Y. Effects of Curing Conditions and Supplementary Cementitious Materials on Autogenous Self-Healing of Early Age Cracks in Cement Mortar. *Crystals* **2021**, *11*, 752. [CrossRef]
50. Alemu, A.S.; Liyew, G.; Lee, B.Y.; Kim, H.-K. Effect of Self-Healing of Cracks in Chloride Ion Diffusion and Corrosion of Engineered Cementitious Composites. *J. Mater. Res. Technol.* **2025**, *35*, 1054–1071. [CrossRef]
51. Abro, F.R.; Buller, A.S.; Ali, T.; Ul-Abdin, Z.; Ahmed, Z.; Memon, N.A.; Lashari, A.R. Autogenous Healing of Cracked Mortar Using Modified Steady-State Migration Test against Chloride Penetration. *Sustainability* **2021**, *13*, 9519. [CrossRef]
52. Park, B.; Choi, Y. Evaluation of Autogenous Healing in Flexural Mortar Members by Chloride Ion Penetration Resistance. *Nanomaterials* **2021**, *11*, 1622. [CrossRef]
53. Sun, R.; Lu, W.; Ma, C.; Tawfek, A.M.; Guan, Y.; Hu, X.; Zhang, H.; Ling, Y.; Šavija, B. Effect of Crack Width and Wet-Dry Cycles on the Chloride Penetration Resistance of Engineered Cementitious Composite (ECC). *Constr. Build. Mater.* **2022**, *352*, 129030. [CrossRef]
54. Van Tittelboom, K.; Gruyaert, E.; Rahier, H.; De Belie, N. Influence of Mix Composition on the Extent of Autogenous Crack Healing by Continued Hydration or Calcium Carbonate Formation. *Constr. Build. Mater.* **2012**, *37*, 349–359. [CrossRef]

55. Reinhardt, H.-W.; Jooss, M. Permeability and Self-Healing of Cracked Concrete as a Function of Temperature and Crack Width. *Cem. Concr. Res.* **2003**, *33*, 981–985. [CrossRef]
56. Yang, Y.; Lepech, M.D.; Yang, E.-H.; Li, V.C. Autogenous Healing of Engineered Cementitious Composites under Wet–Dry Cycles. *Cem. Concr. Res.* **2009**, *39*, 382–390. [CrossRef]
57. Snoeck, D.; Van Tittelboom, K.; Steuperaert, S.; Dubruel, P.; De Belie, N. Self-Healing Cementitious Materials by the Combination of Microfibres and Superabsorbent Polymers. *J. Intell. Mater. Syst. Struct.* **2014**, *25*, 13–24. [CrossRef]
58. Jacobsen, S.; Marchand, J.; Boisvert, L. Effect of Cracking and Healing on Chloride Transport in OPC Concrete. *Cem. Concr. Res.* **1996**, *26*, 869–881. [CrossRef]
59. Edvardsen, C. Water Permeability and Autogenous Healing of Cracks in Concrete. *Mater. J.* **1999**, *96*, 448–454. [CrossRef]
60. Aldea, C.-M.; Song, W.-J.; Popovics, J.S.; Shah, S.P. Extent of Healing of Cracked Normal Strength Concrete. *J. Mater. Civ. Eng.* **2000**, *12*, 92–96. [CrossRef]
61. Pelto, J.; Leivo, M.; Gruyaert, E.; Debbaut, B.; Snoeck, D.; Belie, N.D. Application of Encapsulated Superabsorbent Polymers in Cementitious Materials for Stimulated Autogenous Healing. *Smart Mater. Struct.* **2017**, *26*, 105043. [CrossRef]
62. Wang, Y.; Miao, Y.; Li, Y.; Wang, F.; Mu, S.; Wang, L.; Gao, S.; Lu, Z.; Liu, Z.; Jiang, J. Investigation of the Damage Self-Healing and Chloride-Water Coupled Transport Inhibition Mechanism of Microencapsulated Concrete. *Constr. Build. Mater.* **2024**, *435*, 136838. [CrossRef]
63. Jonkers, H.M.; Thijssen, A.; Muyzer, G.; Copuroglu, O.; Schlangen, E. Application of Bacteria as Self-Healing Agent for the Development of Sustainable Concrete. *Ecol. Eng.* **2010**, *36*, 230–235. [CrossRef]
64. Brasileiro, P.P.F.; Brandão, Y.; Sarubbo, L.; Benachour, M. Self-Healing Concrete: Background, Development, and Market Prospects. *Biointerface Res. Appl. Chem.* **2021**, *11*, 14709–14725. [CrossRef]
65. Gerengi, H.; Kaya, E.; Solomon, M.M.; Snape, M.; Koerdt, A. Advances in the Mitigation of Microbiologically Influenced Concrete Corrosion: A Snapshot. *Materials* **2024**, *17*, 5846. [CrossRef] [PubMed]
66. Javeed, Y.; Goh, Y.; Mo, K.H.; Yap, S.P.; Leo, B.F. Microbial Self-Healing in Concrete: A Comprehensive Exploration of Bacterial Viability, Implementation Techniques, and Mechanical Properties. *J. Mater. Res. Technol.* **2024**, *29*, 2376–2395. [CrossRef]
67. Prajapati, N.K.; Agnihotri, A.K.; Basak, N. Microbial Induced Calcite Precipitation (MICP) a Sustainable Technique for Stabilization of Soil: A Review. *Mater. Today Proc.* **2023**, *93*, 357–361. [CrossRef]
68. Baidya, P.; Dahal, B.K.; Pandit, A.; Joshi, D.R. Bacteria-Induced Calcite Precipitation for Engineering and Environmental Applications. *Adv. Mater. Sci. Eng.* **2023**, *2023*, 2613209. [CrossRef]
69. Luo, M.; Qian, C.; Li, R. Factors Affecting Crack Repairing Capacity of Bacteria-Based Self-Healing Concrete. *Constr. Build. Mater.* **2015**, *87*, 1–7. [CrossRef]
70. Tziviloglou, E.; Wiktor, V.; Jonkers, H.M.; Schlangen, E. Bacteria-Based Self-Healing Concrete to Increase Liquid Tightness of Cracks. *Constr. Build. Mater.* **2016**, *122*, 118–125. [CrossRef]
71. Ling, H.; Qian, C. Effects of Self-Healing Cracks in Bacterial Concrete on the Transmission of Chloride during Electromigration. *Constr. Build. Mater.* **2017**, *144*, 406–411. [CrossRef]
72. Mohsenzadeh, A.; Aflaki, E.; Gowthaman, S.; Nakashima, K.; Kawasaki, S.; Ebadi, T. A Two-Stage Treatment Process for the Management of Produced Ammonium by-Products in Ureolytic Bio-Cementation Process. *Int. J. Environ. Sci. Technol.* **2022**, *19*, 449–462. [CrossRef]
73. Jin, C.; Yu, R.; Shui, Z. Fungi: A Neglected Candidate for the Application of Self-Healing Concrete. *Front. Built Environ.* **2018**, 4. [CrossRef]
74. Elkhateeb, W.; Elnahas, M.O.; Daba, G. Fungal Calcium Carbonate Mineralization as a Microbial Approach for Concrete Self-Healing. *Geomicrobiol. J.* **2022**, *39*, 631–636. [CrossRef]
75. Luo, J.; Chen, X.; Crump, J.; Zhou, H.; Davies, D.G.; Zhou, G.; Zhang, N.; Jin, C. Interactions of Fungi with Concrete: Significant Importance for Bio-Based Self-Healing Concrete. *Constr. Build. Mater.* **2018**, *164*, 275–285. [CrossRef]
76. Zhang, X.; Fan, X.; Li, M.; Samia, A.; Yu, X. (Bill) Study on the Behaviors of Fungi-Concrete Surface Interactions and Theoretical Assessment of Its Potentials for Durable Concrete with Fungal-Mediated Self-Healing. *J. Clean. Prod.* **2021**, *292*, 125870. [CrossRef]
77. Khushnood, R.A.; Ali, A.M.; Faraz Bhatti, M.; Ahmed Khan, H. Self-Healing Fungi Concrete Using Potential Strains *Rhizopus oryzae* and *Trichoderma longibrachiatum*. *J. Build. Eng.* **2022**, *50*, 104155. [CrossRef]
78. Youssa Tchamou, L.K.; Xue, C. Effect of MICP on Reinforcement Corrosion of Cement Concrete Exposed to the Marine Environment. *Discov. Civ. Eng.* **2025**, *2*, 47. [CrossRef]
79. Chang, J.; Yang, D.; Lu, C.; Shu, Z.; Deng, S.; Tan, L.; Wen, S.; Huang, K.; Duan, P. Application of Microbially Induced Calcium Carbonate Precipitation (MICP) Process in Concrete Self-Healing and Environmental Restoration to Facilitate Carbon Neutrality: A Critical Review. *Environ. Sci. Pollut. Res.* **2024**, *31*, 38083–38098. [CrossRef]
80. Adhikary, S.K.; Rathod, N.; Adhikary, S.D.; Kumar, A.; Perumal, P. Chemical-Based Self-Healing Concrete: A Review. *Discov. Civ. Eng.* **2024**, *1*, 119. [CrossRef]

81. Matinfar, M.; Nychka, J.A. A Review of Sodium Silicate Solutions: Structure, Gelation, and Syneresis. *Adv. Colloid Interface Sci.* **2023**, *322*, 103036. [CrossRef] [PubMed]
82. Roig-Flores, M.; Pirritano, F.; Serna, P.; Ferrara, L. Effect of Crystalline Admixtures on the Self-Healing Capability of Early-Age Concrete Studied by Means of Permeability and Crack Closing Tests. *Constr. Build. Mater.* **2016**, *114*, 447–457. [CrossRef]
83. Zhang, Y.; Wang, R.; Ding, Z. Influence of Crystalline Admixtures and Their Synergetic Combinations with Other Constituents on Autonomous Healing in Cracked Concrete—A Review. *Materials* **2022**, *15*, 440. [CrossRef] [PubMed]
84. Ferrara, L.; Van Mullem, T.; Alonso, M.C.; Antonaci, P.; Borg, R.P.; Cuenca, E.; Jefferson, A.; Ng, P.-L.; Peled, A.; Roig-Flores, M.; et al. Experimental Characterization of the Self-Healing Capacity of Cement Based Materials and Its Effects on the Material Performance: A State of the Art Report by COST Action SARCOS WG2. *Constr. Build. Mater.* **2018**, *167*, 115–142. [CrossRef]
85. Sisomphon, K.; Copuroglu, O.; Koenders, E.A.B. Self-Healing of Surface Cracks in Mortars with Expansive Additive and Crystalline Additive. *Cem. Concr. Compos.* **2012**, *34*, 566–574. [CrossRef]
86. Gilford, J.; Hassan, M.M.; Rupnow, T.; Barbato, M.; Okeil, A.; Asadi, S. Dicyclopentadiene and Sodium Silicate Microencapsulation for Self-Healing of Concrete. *J. Mater. Civ. Eng.* **2014**, *26*, 886–896. [CrossRef]
87. Van Belleghem, B.; Kessler, S.; Van den Heede, P.; Van Tittelboom, K.; De Belie, N. Chloride Induced Reinforcement Corrosion Behavior in Self-Healing Concrete with Encapsulated Polyurethane. *Cem. Concr. Res.* **2018**, *113*, 130–139. [CrossRef]
88. Comensoli, L.; Albini, M.; Kooli, W.; Maillard, J.; Lombardo, T.; Junier, P.; Joseph, E. Investigation of Biogenic Passivating Layers on Corroded Iron. *Materials* **2020**, *13*, 1176. [CrossRef]
89. Lou, Y.; Chang, W.; Cui, T.; Wang, J.; Qian, H.; Ma, L.; Hao, X.; Zhang, D. Microbiologically Influenced Corrosion Inhibition Mechanisms in Corrosion Protection: A Review. *Bioelectrochemistry* **2021**, *141*, 107883. [CrossRef]
90. White, G.F.; Shi, Z.; Shi, L.; Wang, Z.; Dohnalkova, A.C.; Marshall, M.J.; Fredrickson, J.K.; Zachara, J.M.; Butt, J.N.; Richardson, D.J.; et al. Rapid Electron Exchange between Surface-Exposed Bacterial Cytochromes and Fe(III) Minerals. *Proc. Natl. Acad. Sci. USA* **2013**, *110*, 6346–6351. [CrossRef]
91. Long, X.; Okamoto, A. Outer Membrane Compositions Enhance the Rate of Extracellular Electron Transport via Cell-Surface MtrC Protein in Shewanella Oneidensis MR-1. *Bioresour. Technol.* **2021**, *320*, 124290. [CrossRef]
92. Volkland, H.-P.; Harms, H.; Kaufmann, K.; Wanner, O.; Zehnder, A.J.B. Repair of Damaged Vivianite Coatings on Mild Steel Using Bacteria. *Corros. Sci.* **2001**, *43*, 2135–2146. [CrossRef]
93. Elsener, B.; Büchler, M.; Stalder, F.; Böhni, H. Migrating Corrosion Inhibitor Blend for Reinforced Concrete: Part 2—Inhibitor as Repair Strategy. *Corrosion* **2000**, *56*, 727–732. [CrossRef]
94. Song, Y.; Liu, J.; Wang, H.; Shu, H. Research Progress of Nitrite Corrosion Inhibitor in Concrete. *Int. J. Corros.* **2019**, *2019*, 3060869. [CrossRef]
95. Cao, Q.; Kang, S.; Lu, C.; Sun, D.; Li, J.; Chen, H.; Li, X. Properties and Corrosion Resistance Mechanism of a Self-Healing Octadecyl Amine Loaded Ethyl Cellulose Microcapsule Coatings Loaded with Epoxy Resin. *Sci. Rep.* **2025**, *15*, 1386. [CrossRef] [PubMed]
96. Fedrizzi, L.; Azzolini, F.; Bonora, P.L. The Use of Migrating Corrosion Inhibitors to Repair Motorways' Concrete Structures Contaminated by Chlorides. *Cem. Concr. Res.* **2005**, *35*, 551–561. [CrossRef]
97. Berke, N.S.; Hicks, M.C. Predicting Long-Term Durability of Steel Reinforced Concrete with Calcium Nitrite Corrosion Inhibitor. *Cem. Concr. Compos.* **2004**, *26*, 191–198. [CrossRef]
98. Lee, H.-S.; Saraswathy, V.; Kwon, S.-J.; Karthick, S. Corrosion Inhibitors for Reinforced Concrete: A Review. In *Corrosion Inhibitors, Principles and Recent Applications*; Aliofkhazraei, M., Ed.; InTech: London, UK, 2018; ISBN 978-953-51-3917-1.
99. Wu, M.; Ma, H.; Shi, J. Beneficial and Detrimental Effects of Molybdate as an Inhibitor on Reinforcing Steels in Saturated $Ca(OH)_2$ Solution: Spontaneous Passivation. *Cem. Concr. Compos.* **2021**, *116*, 103887. [CrossRef]
100. Gojević, A.; Ducman, V.; Netinger Grubeša, I.; Baričević, A.; Banjad Pečur, I. The Effect of Crystalline Waterproofing Admixtures on the Self-Healing and Permeability of Concrete. *Materials* **2021**, *14*, 1860. [CrossRef]
101. Snoeck, D. Superabsorbent Polymers to Seal and Heal Cracks in Cementitious Materials. *RILEM Tech. Lett.* **2018**, *3*, 32–38. [CrossRef]
102. Van Tittelboom, K.; De Belie, N. Self-Healing in Cementitious Materials—A Review. *Materials* **2013**, *6*, 2182–2217. [CrossRef]
103. Zhang, W.; Zheng, Q.; Ashour, A.; Han, B. Self-Healing Cement Concrete Composites for Resilient Infrastructures: A Review. *Compos. Part B Eng.* **2020**, *189*, 107892. [CrossRef]
104. Wang, Y.; Pham, D.T.; Ji, C. Self-Healing Composites: A Review. *Cogent Eng.* **2015**, *2*, 1075686. [CrossRef]
105. Jiang, L.; Wu, M.; Du, F.; Chen, D.; Xiao, L.; Chen, W.; Du, W.; Ding, Q. State-of-the-Art Review of Microcapsule Self-Repairing Concrete: Principles, Applications, Test Methods, Prospects. *Polymers* **2024**, *16*, 3165. [CrossRef]
106. Reda, M.A.; Chidiac, S.E. Performance of Capsules in Self-Healing Cementitious Material. *Materials* **2022**, *15*, 7302. [CrossRef]
107. Osibodu, S.J.; Adeyinka, A.M.; Mbelu, O.V. Phase Change Material Integration in Concrete for Thermal Energy Storage: Techniques and Applications in Sustainable Building. *Sustain. Energy Res.* **2024**, *11*, 45. [CrossRef]

108. Sukumaran, A.; Johnpaul, V.; Balasundaram, N.; Senthil Kumar, S. Bacterial Concrete: The Future of Self-Healing and Sustainable Infrastructure. *Methods X* **2025**, *15*, 103569. [CrossRef] [PubMed]
109. Pooja, K.; Tarannum, N. Self-Healing Concrete: A Path towards Advancement of Sustainable Infrastructure. *Discov. Appl. Sci.* **2025**, *7*, 703. [CrossRef]
110. Cappellesso, V.G.; Van Mullem, T.; Gruyaert, E.; Van Tittelboom, K.; De Belie, N. Self-Healing Concrete with a Bacteria-Based or Crystalline Admixture as Healing Agent to Prevent Chloride Ingress and Corrosion in a Marine Environment. *Dev. Built Environ.* **2024**, *19*, 100486. [CrossRef]
111. Liu, Y.; Shi, J. Exploring a Feasible Inhibitor-Coating Protective System for Corrosion Protection of Steel in Mortar. *Cem. Concr. Compos.* **2025**, *161*, 106109. [CrossRef]
112. Ma, Y.; Wang, S.; Li, M.; Wang, G.; Liu, J.; Gao, Y.; Wang, P.; Zhang, Z. Degradation Behavior and Self-Healing Mechanism of Force-Cl^- Triggered Microcapsule/Cementitious Composites. *Cem. Concr. Compos.* **2025**, *157*, 105951. [CrossRef]
113. Qian, C.; Wu, Z.; Ren, X.; Fan, W.; Qu, J. Study on Crack Repair Effect of Microbial Self–Healing Concrete and Corrosion Inhibition of Steel Bar. *Structures* **2024**, *70*, 107810. [CrossRef]
114. Wang, X.F.; Yang, Z.H.; Fang, C.; Wang, W.; Liu, J.; Xing, F. Effect of Carbonate-Containing Self-Healing System on Properties of a Cementitious Composite: Fresh, Mechanical, and Durability Properties. *Constr. Build. Mater.* **2020**, *235*, 117442. [CrossRef]
115. Erşan, Y.Ç.; Verbruggen, H.; De Graeve, I.; Verstraete, W.; De Belie, N.; Boon, N. Nitrate Reducing $CaCO_3$ Precipitating Bacteria Survive in Mortar and Inhibit Steel Corrosion. *Cem. Concr. Res.* **2016**, *83*, 19–30. [CrossRef]
116. Kanwal, M.; Adnan, F.; Khushnood, R.A.; Jalil, A.; Khan, H.A.; Wattoo, A.G.; Rasheed, S. Biomineralization and Corrosion Inhibition of Steel in Simulated Bio-Inspired Self-Healing Concrete. *J. Build. Eng.* **2024**, *82*, 108224. [CrossRef]
117. Tang, Y.; Li, Y.; Liu, X.; Chen, W.; Schollbach, K.; Chen, W. Biomimetic-Induced Hydroxyapatite for Rebar Corrosion Mitigation in Self-Healing Concrete Beam. *J. Build. Eng.* **2024**, *84*, 108666. [CrossRef]

Disclaimer/Publisher's Note: The statements, opinions and data contained in all publications are solely those of the individual author(s) and contributor(s) and not of MDPI and/or the editor(s). MDPI and/or the editor(s) disclaim responsibility for any injury to people or property resulting from any ideas, methods, instructions or products referred to in the content.